HELSINGIN YLIOPISTO
HELSINGFORS UNIVERSITET
UNIVERSITY OF HELSINKI

Glutamine Control of Intestinal Stem Cells in *Drosophila melanogaster*

Arto I. Viitanen

Master's thesis

University of Helsinki

Department of Biosciences

Master's Programme in Genetics and Molecular Biosciences

May 2019

HELSINGIN YLIOPISTO
HELSINGFORS UNIVERSITET
UNIVERSITY OF HELSINKI

Tiedekunta – Fakultet – Faculty	Koulutusohjelma – Utbildingsprogram – Degree Programme
Biological and Environmental Biosciences	Genetics and Molecular Biosciences

Tekijä – Författare – Author
Arto Ilmari Viitanen

Työn nimi – Arbetets titel – Title
Glutamine Control of Intestinal Stem Cells in *Drosophila melanogaster*

Oppiaine/Opintosuunta – Läroämne/Studieinriktning – Subject/Study track
Genetics and Genomics

Työn laji – Arbetets art – Level	Aika – Datum – Month and year	Sivumäärä – Sidoantal – Number of pages
Master's Thesis	May, 2019	52+17

Tiivistelmä – Referat – Abstract
The intestinal stem cells (ISC) are responsible for the regeneration of the intestine epithelial barrier after acute injury and for the replenishment of its cells overall. How the ISC activation and resulting proliferation is controlled is complex and still under study. The ISCs of the midgut, which is the functional analogue to mammalian small intestine, are also highly responsive to changes in nutrition, and with proper methodologies it is possible to study the effects of diet on stem cell activation. The metabolic flux of the nutritional components of the diet can then shed light on which metabolic pathways are necessary for nutrient-dependent proliferation. One nutrient that has garnered interest is glutamine (Gln). It is well established that glutamine supplementation can in parenterally fed patients diminish intestinal barrier atrophy, extend the time the patient can be kept under the regime, and increase survivability of critically ill patients. Consequently, glutamine or its downstream metabolites may have stem cell activating characteristics. However, the exact regulatory mechanisms and specific effects of Gln are not well known, and studies have found contradictory results on the beneficial effects of Gln supplementation. Glutamine itself is a conditionally essential amino acid that has a variety of functions: it is an important source of nitrogen and cellular energy and contributes carbon into the tricarboxylic acid cycle (TCA) and is involved in protein and nucleotide synthesis.

In this thesis, the effects of Gln supplementation on the cell populations of *D. melanogaster* were studied via microscopy and computational analysis. Cross-breeds of fruit fly were established to lineage label the ISC with a GAL4/UAS driver system. Confocal microscope was used to image the midguts which were then analysed with Imaris software. A novel analysis method was developed to study population changes and varying features of the cells in the midgut in an unprecedented region-by-region bulk analysis. Earlier studies into nutrient control of ISC have had limited focus within the midgut and might have consequently given a restricted view of ISC activation. This new Longitudinal Analysis of Midgut (LAM) can be utilized in a diverse set of further studies to describe conditional variation within midgut, and possibly other tissues.

Gln was found to increase total cell numbers to comparable levels with well-fed midguts, and to drive limited endoreplication in enterocytes. Lineage labelled cell population grew primarily in the R3 and R4 regions of the midgut. Additionally, enteroendocrine cells (EE) were greatly increased in the posterior part of R3 but had conceivable minor increases along the whole length of the midgut. Improved nutrition was also found to affect the proportions of the midgut, presenting itself as elongated posterior and stunted anterior.

Overall, the pipeline and analysis method established during this study enable more expeditious research of effects of other nutritional components and allows for study of effects of other mechanisms, for example how gene knock-downs or altered gene activities affect cell populations of the midgut.

Avainsanat – Nyckelord – Keywords
Drosophila, midgut, intestinal stem cell, glutamine, nutrition, computational biology

Ohjaaja tai ohjaajat – Handledare – Supervisor or supervisors
Jaakko Mattila, PhD (primary supervisor) & Ville Hietakangas, PhD

Säilytyspaikka – Förvaringställe – Where deposited

Muita tietoja – Övriga uppgifter – Additional information

HELSINGIN YLIOPISTO
HELSINGFORS UNIVERSITET
UNIVERSITY OF HELSINKI

Tiedekunta – Fakultet – Faculty	Koulutusohjelma – Utbildingsprogram – Degree Programme	
Bio- ja ympäristötieteellinen tiedekunta	Genetiikka ja molekulaariset biotieteet	
Tekijä – Författare – Author		
Arto Ilmari Viitanen		
Työn nimi – Arbetets titel – Title		
Glutamiini *Drosophila melanogaster*in suolen kantasolujen säätelyssä		
Oppiaine/Opintosuunta – Läroämne/Studieinriktning – Subject/Study track		
Genetiikka ja genomiikka		
Työn laji – Arbetets art – Level	Aika – Datum – Month and year	Sivumäärä – Sidoantal – Number of pages
Maisterintutkielma	Toukokuu, 2019	52+17

Tiivistelmä – Referat – Abstract

Nisäkkäiden ohutsuolta vastaavan *Drosophil*an keskisuolen kantasolut ovat sen ainoina jakautuvina soluina vastuussa epiteelin solujen täydentämisestä, niin reaktiona vaurioitumiseen kuin normaaliin soluvaihtuvuuteen. Kantasolujen aktivoitumisen säätelymekanismit ja niistä johtuva proliferaatio ovat monimutkaisia, sekä edelleen tutkimuksen kohteina. Keskisuoli myös reagoi voimakkaasti ruoan ravintoaineisiin, ja tarkkaan kontrolloiduilla tutkimusasetelmilla kyetään selvittämään miten yksittäinen ravintoaine vaikuttaa kantasolujen toimintaan. Mikäli vaikutus löydetään, kyseisen ravintoaineen metaboliareittien tutkimus saattaa antaa uutta tietoa keskisuolen ja kantasolujen säätelystä. On todettu, että aminohappo glutamiini voi parenteraaliseen ruokinnan lisänä ehkäistä suolistoesteen surkastumista, lisätä kriittisesti sairaiden potilaiden selviytymistä, sekä pidentää aikaa, jolloin potilasta voidaan pitää ruokinnassa. Glutamiini on suoliston soluille tärkeä energian lähde, joka toimii myös hiilen lähteenä sitruunahappokierrossa ja elinten välisenä typenkuljettajana. Lisäksi glutamiini on myös osallisena proteiinien sekä nukleotidien synteesissä.

Tutkielmassa tarkastellaan glutamiinilisän vaikutusta keskisuolen solupopulaatioihin sekä niiden ominaisuuksiin konfokaalimikroskopian ja tietokonelaskennan keinoin. Mikroskopiaa varten perustettiin Gal4/UAS-järjestelmään pohjautuva sukujuurijäljitys risteyttämällä kaksi *Drosophila*-kantaa, sekä leimattiin kaksi solutyyppiä fluoresoivilla aineilla. Kuvat analysoitiin ensin Imaris-ohjelmalla ja sen jälkeen tutkielmaa varten kehitetyllä analyysimetodilla, joka mahdollistaa keskisuolen eri alueiden kokonaisvaltaisen tarkastelun. Aiemmat ravintoainesäätelyä tarkastelleet tutkimukset ovat pääasiallisesti keskittyneet vain tiettyihin keskisuolen osa-alueisiin, mistä johtuen kokonaiskuva säätelystä on voinut jäädä vajavaiseksi. Valmistunutta “Longitudinal Analysis of Midgut”-menetelmää (LAM) voidaan jatkossa hyödyntää uusien ravintoaineiden ja muiden suolen soluihin vaikuttavien tekijöiden tutkimiseen.

Glutamiinilisän havaittiin kasvattavan keskisuolten kokonaissolumääriä lähes samalle tasolle kuin eläimillä, joita oli ruokittu kaikkia tarpeellisia ravintoaineita sisältävällä dieetillä. Sukujuurileimattujen solujen havaittiin lisääntyvän pääasiassa R3- ja R4-alueilla. Suurin solumäärien kasvu havaittiin enteroendokriinisoluilla posterioorisessa R3:ssa, mutta merkittävää kasvua oli lähes koko keskisuolen alueella. Ravinnon huomattiin myös muuttavan keskisuolen eri osien mittasuhteita: anterioorinen puoli lyheni ja posterioorinen pidentyi. Viitteitä löytyi myös endoreplikaation aktivoitumisesta enterosyyteissä.

Tutkielman aikana muodostunut analyysiprotokolla sekä uusi tietokonelaskennallinen menetelmä mahdollistavat tulevaisuudessa nopeamman ravintoaineiden vaikutuksien tutkimuksen keskisuolessa. Menetelmä on myös hyödynnettävissä monenlaisiin muihin tutkimuksiin jotka vaikuttavat suoliston solukantoihin.

Avainsanat – Nyckelord – Keywords

Drosophila, keskisuoli, suoliston kantasolut, glutamiini, ravitsemus, laskennallinen biologia

Ohjaaja tai ohjaajat – Handledare – Supervisor or supervisors

Jaakko Mattila, FT (Ensisijainen ohjaaja) & Ville Hietakangas, FT

Säilytyspaikka – Förvaringställe – Where deposited

Muita tietoja – Övriga uppgifter – Additional information

HELSINGIN YLIOPISTO
HELSINGFORS UNIVERSITET
UNIVERSITY OF HELSINKI

Acknowledgements

My foremost gratitude goes to Jaakko Mattila and Ville Hietakangas. Thank you for taking me under your *Drosophila* wing, offering me a position at the lab, and easing me into the study of fruit fly. I would also like to thank everyone else at the lab who has bounced ideas with me. As for my parents, thank you for supporting me through these past school years, as balancing studies and work can get rough. Last, I begrudgingly impart my gratitude towards my friends just for existing, even though you have tried your best to offer alternative activities to studying.

HELSINGIN YLIOPISTO
HELSINGFORS UNIVERSITET
UNIVERSITY OF HELSINKI

Table of Contents

HELSINGIN YLIOPISTO
HELSINGFORS UNIVERSITET
UNIVERSITY OF HELSINKI

List of Terms and Abbreviations

Act	Actin
AKG	α-ketoglutarate
DF	Pandas DataFrame –object
Dl	Delta
Dpp	Decapentaplegic
EB	Enteroblast
EC	Enterocyte
EE	Enteroendocrine cells
EGF	Epidermal growth factor
EGFR	Epidermal growth factor receptor
Esg	Escargot
Esg F/O	Escargot Flip-out
Flp	flippase
FRT	Flippase recognition target
Gfat	Glutamine fructose-6-phosphate amidotransferase
GFP	Green fluorescent protein
ID	Imaris object identifier number
IGF	Insulin-like growth factor
ILP3	Insulin-like peptide 3
InR	Insulin-like receptor
ISC	Intestinal stem cell
Lab	Labial
LAM	Longitudinal Analysis of Midgut
MWW	Mann-Whitney-Wilcoxon U test
NA	Numerical aperture
PBS	Phosphate buffered saline
PBT	PBS with Triton
PFA	Paraformaldehyde solution
PM	Peritrophic matrix
Pros	Prospero

sCMOS	scientific complementary metal-oxide-semiconductor (image sensor)
SDCM	Spinning disc confocal microscope
SIM	Structured illumination microscopy
Su(H)	Suppressor of Hairless
TCA	Tricarboxylic acid cycle
TF	Transcription factor
Tub	Tubulin
UAS	Upstream activating sequence
Upd1	Unpaired1, a JAK-STAT ligand
VM	Visceral muscle cells
Vn	Vein, an EGFR ligand

1. Introduction

The diet of an organism can have far-reaching consequences on the well-being and functionality of the intestine (Miguel-Aliaga et al., 2018; Shaw et al., 2012). Many organisms that are naturally intermittent feeders such as *Drosophila melanogaster*, known by the common name fruit fly, have the remarkable ability to increase proliferation rate and gene expression in order to grow in size when nutrition is abundant (Miguel-Aliaga et al., 2018). Conversely, in nutrient-depleted conditions the division rate can be driven down and many functions of the intestine can be ceased (Choi et al., 2011; O'Brien et al., 2011). At the heart of this adaptability are various nutrient-sensing and signalling pathways that can regulate cell activity and function (Choi et al., 2011; Mattila et al., 2018; O'Brien et al., 2011). Arguably, the most important of these cells are the intestinal stem cells (ISC) which are the only mitotic cells within the *Drosophila* intestine, and are therefore in control of revitalising the epithelium after injury, infection, and degradation (Micchelli and Perrimon, 2006).

The *Drosophila* midgut, which is comparable to the human small intestine, has become one of the key models in studying how nutrition affects cellular functions. Due to its compartmentalised structure where each have unique identities, many regulatory mechanisms and pathways can be studied in a more controlled manner (Buchon et al., 2013; Marianes and Spradling, 2013). These regions within the midgut are characterised by their differing gene expression patterns, varying histology, and separate physiological functions. While the regions are individualised, together they form a functional whole: from the anterior to the posterior all nutrients are systematically broken down and then absorbed (Lemaitre and Miguel-Aliaga, 2013; Miguel-Aliaga et al., 2018). In addition to the stem cells, the midgut is populated by four primary cell types: progenitor cells called enteroblasts (EB), enteroendocrine cells (EE), enterocytes (EC), and visceral muscle cells (VM) (Hung et al., 2018).

One of the key pathways recognized for controlling cell and organ growth is the insulin/IGF pathway, which ties systemic signalling to local and cell intrinsic signalling (O'Brien et al., 2011; Vinayagam et al., 2016). However, studies into insulin signalling-induced proliferation have obtained contradictory results; activation of the signalling has been found to lead to either increased or reduced growth, and the regulation of the outcome has been ambiguous (Choi et al., 2011; Mattila et al., 2018). Revealing the true mechanisms behind nutrition and stem cell activation is crucial for our

understanding of regulation of homeostasis and epithelial renewing. This knowledge would most likely be transferrable to humans as many pathways have been found to be highly conserved, and might consequently give us new insights into many intestinal diseases from Crohn's disease to obesity (Apidianakis and Rahme, 2011). Moreover, as cancerous cells obtain stem cell-like qualities, determining how stem cells are regulated could provide new insight into how tumours are formed and maintained, and might ultimately reward us with new targets for treatment (Mihaylova et al., 2014).

One possible way to study nutrient-dependent pathways is by altering diet regimens of the model organism and then quantifying any emerging effects. For this thesis, the effects of glutamine (Gln) supplementation on midgut cell populations and other cell-specific characteristics were studied. Glutamine is of interest for the study of stem cells, as it has been known to prevent deterioration of gut permeability and regenerate atrophied intestinal barrier in critically-ill patients on parenteral nutrition (van der Hulst et al., 1993; Miller, 1999). Moreover, recent research revealed one glutamine metabolism downstream-pathway, i.e. the hexosamine biosynthesis pathway, to have growth-inducing regulatory effect on insulin signalling activity (Mattila et al., 2018).

Earlier studies into stem cell activity and regulation have typically focused either on specific regions of the midgut or on whole midgut with insufficient regional resolution (Choi et al., 2011; Zeng and Hou, 2015). As it is known that the regions have distinct identities, this limited research focus can lead lacklustre picture of the whole and can reveal inconsistent results. Recent advances in confocal microscopy and computation have made it possible to image whole *Drosophila* organs in a time-frame reasonable for bulk analysis (Jonkman and Brown, 2015; Langhorst et al., 2009). While the whole-midgut images are relatively easily obtained, the analysis throughput is limited by current work-intensive analytical methods. By developing proper tools, these images could be used to analyse the midgut in a more comprehensive way. The possibility of high-resolution bulk analysis of whole-midgut images is very promising for the study of region-specific and midgut-wide effects of nutrition and the regulation of nutrient-dependent pathways.

In this thesis, the effects of glutamine supplementation on midgut were studied in comparison to starved and well-fed flies. Lineage tracing was used in conjunction with cell type-specific fluorescent staining to obtain whole-midgut spinning disc confocal images with distinguishable cell populations. A novel Python-based bulk analysis method was developed to overcome the current restrictions on

midgut-wide image analysis. The developed analysis pipeline reduces the dimensionality of the image data, consequently allowing a dependable and high-resolution quantification of cellular populations and cell-specific characteristics along the whole length of the midgut. The aim of the research was in characterising the effects of glutamine supplementation and in developing the methodology.

2. Review of the Literature

2.1 *Drosophila melanogaster*

Drosophila melanogaster, or fruit fly, are insects belonging to the *Diptera* family, commonly known as flies. They are spread on every continent and live and feed on decomposing fruit and yeast within. Fruit fly has become a valuable model organism in multiple areas of research, including stem cell regulation (Cox et al., 2017; Miguel-Aliaga et al., 2018; Sokolowski, 2001). Compared to mammalian model organisms, the *Drosophila* genome is shorter and contains less genes, which is indicative of less redundancy and can present itself as relatively simplified pathways (Hughes et al., 2012; Zacharioudaki and Bray, 2014). As a result, studies on *Drosophila* may uncover fundamental mechanisms of various cellular processes found also in humans. Moreover, the ease of rearing, high rate of egg-laying, and relatively short lifespan renders experimental design easier and experiments briefer. While the fruit fly shares most of its genes with humans, their genome only contains four chromosomes: the sex chromosomes X/Y, and autosomes 2, 3, and 4 (Myers et al., 2000). Many disease-associated sequences of humans can also be found in the *Drosophila* genome, and studying how these function in the model organism can reveal real insights in human pathologies (Apidianakis and Rahme, 2011; Reiter et al., 2001). The *Drosophila* midgut has become increasingly studied since the discovery of its inhabiting stem cells (Micchelli and Perrimon, 2006; Ohlstein and Spradling, 2006). The mechanisms and transcriptional regulation within midgut can shed light into gastrointestinal diseases and obesity in humans, but also how nutrient control and stem cell regulation functions.

2.2 The Midgut

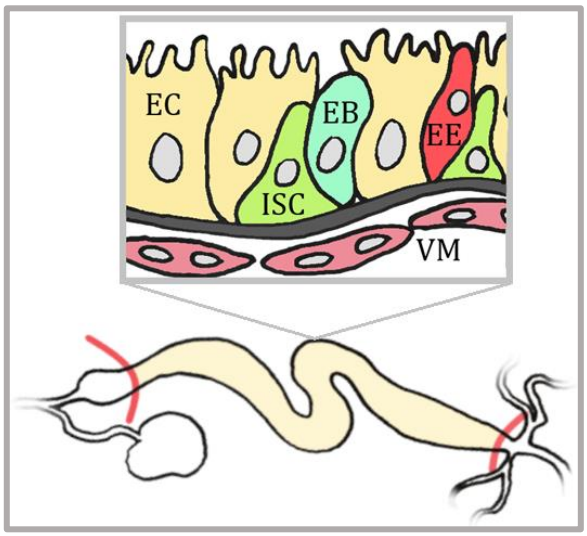

Fig. 1. The* Drosophila *midgut and the architecture of the epithelium. *On the left side before the midgut (coloured) is the foregut, including the crop, a food storage found in adults. On the posterior side of midgut is the hindgut, with malpighian tubules, i.e. the* Drosophila *analogue to kidneys. Enterocytes (EC), intestinal stem cells (ISC), enteroendocrine cells (EE), and enteroblasts (EB) populate the midgut, which is surrounded by visceral muscle cells (VM).*

The *Drosophila* midgut is the functional analogue of the mammalian small intestine, i.e. it is devoted to food digestion and nutrient absorption, and is the primary digestive organ (Buchon et al., 2013). In contrast to the morphology of the mammalian intestine, the *Drosophila* midgut does not form crypts of Lieberkühn, the intestinal glands where new epithelial cells are formed, or even crypt-like structures (Clevers, 2013). Instead, the midgut consists of a single cell layer, a sleeve-like pseudostratified epithelium with progenitor cells distributed all along it (Fig. 1). On the basal side, the epithelium is surrounded by nerves and visceral muscle cells, but also tracheae, or respiratory tubes (Lemaitre and Miguel-Aliaga, 2013). Nutrient absorption is not the only function of the midgut: enteroendocrine cells within it contribute to the endocrine signalling system, and as an epithelial tissue, the midgut is introduced to a variety of outside chemicals and infectious agents, and as a result serves an additional purpose as a barrier. In addition to the epithelial barrier, the intestines of insects are protected by the peritrophic matrix (PM) (Hegedus et al., 2008; Lemaitre and Miguel-Aliaga, 2013). The PM is a chitinous lattice that is excreted from the proventriculus, i.e. the cardia between foregut and midgut. Peristalsis of the gut forces the PM towards the posterior and accordingly coats the midgut in a carbohydrate-rich lining, forming a functionally similar protective barrier as the vertebrate digestive tract mucus.

As in the mammalian counterpart, the midgut has been defined to contain multiple morphologically and functionally distinctive subregions marked by their varying cell populations and transcriptomes (Buchon et al., 2013; Dutta et al., 2015). Each of these regions are comprised of four principal cell types: multipotent intestinal stem cells, enteroendocrine cells, enterocytes, and post-mitotic progenitor enteroblasts. However, these primary cell types can be further divided into subpopulations

based on their varying gene activities. A recent study by Hung *et al* found 12 distinct clusters of midgut epithelial cells with single-cell RNA-sequencing (Hung et al., 2018). The EC had the most numerous representation within these clusters with a total of eight transcriptionally separate populations, which is in accordance with the existing literature showing that the ECs have regional differences in the expression of various digestive enzyme coding genes (Lemaitre and Miguel-Aliaga, 2013; Miguel-Aliaga et al., 2018).

2.2.1 Regions of the Midgut

The midgut can be divided into three compartments due to their recognizable morphology: the anterior, middle, and posterior regions (Fig. 2). However, with recent advances in the accessibility and power of computational molecular biology methods, e.g. RNA and DNA sequencing, a more detailed picture of the midgut has emerged. In a 2013 journal article, Buchon *et al.* described six primary regions of the midgut that have become the standard classification (Buchon et al., 2013). All these regions have differing metabolic and digestive functionalities. Additionally, they can be characterized by their varying cell populations and distinctive transcriptomes (Dutta et al., 2015; Hung et al., 2018). These regional transcriptomes are not only defined by changing proportions of major cell types, but these cell types attain regional identities in order to perform their functionality. The regionalization along the midgut is controlled by numerous transcription factors including e.g. Labial and Wnt (Miguel-Aliaga et al., 2018). For example, Wnt reporter Fz3-RFP has been found to align with regional gene expression patterns, suggesting that Wnt has organizational role (Buchon et al., 2013; Dutta et al., 2015). The regional boundaries are not always exact to the eye, and the transcriptional levels can in some cases change in gradients, but the identities are evident from region

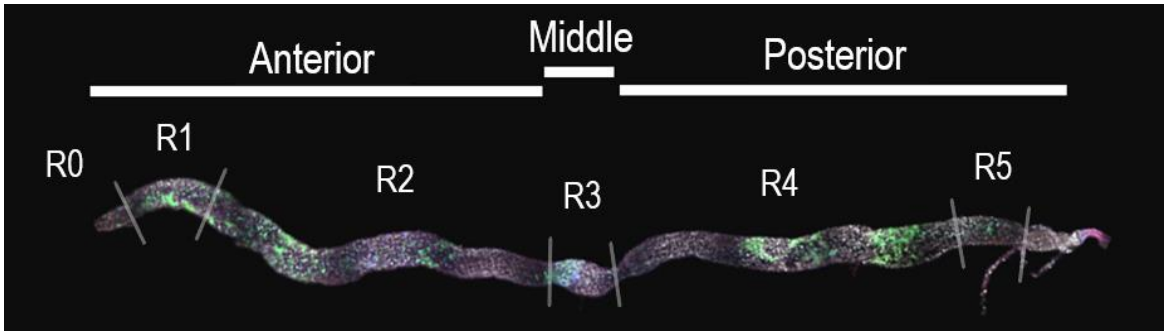

Fig. 2. The regions of the adult midgut. *The histological division into anterior, middle, and posterior regions, and the modern primary R0–5 region division as described by Buchon* et al. *Not all the region changes are clear to the eye, but closer inspection can distinguish narrow epithelial barriers. Moreover, regional transcriptomes are divergent.*

to region (Lemaitre and Miguel-Aliaga, 2013). Furthermore, it is known that stem cells within the regions do not for the most part contribute progeny to adjacent regions (Marianes and Spradling, 2013). Overall, the evidence suggests that the individualities of the regions are precisely controlled.

The six regions, named R0–R5 (Fig. 2B), can be further divided into 10–14 subregions (Buchon et al., 2013). An alternative compartmentalisation offered by Marianes and Spradling divided the midgut into three anterior (A1–3), four posterior (P1–4), and three middle regions (Copper, Large Flat Cell, and Iron) based on various properties (Marianes and Spradling, 2013). The R0 to R5 compartmentalisation was used for this thesis for consistent reference to regions.

The full functionalities of the described regions are still under study, but it is known that they have variable physicochemical properties, proliferation rates, cell subtypes, and cell composition. Most distinct of these is the R3-region. As described by Buchon *et al.*, it has a distinct expression profile and seems to act as a kind of symmetry centre, i.e. the R1-R2 are more alike to R4-R5 than R3 transcriptionally (Buchon et al., 2013). The R3 also contains the R3ab-subregion, also known as "stomach" or copper cell region, that contains a distinct population of ISC called the gastric stem cells (GSSC) that are generally quiescent, but can become activated in response to challenges (Strand and Micchelli, 2011). The subregion is also characterised by the namesake copper cells (see 2.3.2 enterocytes). Due to the boundary-restricted expression patterns and variable cell populations, the regions and subregions can be considered as functional units. In addition to the various regulatory pathways, the regional identities and functionalities are in part maintained by the proliferative intestinal stem cells.

2.3 Stem Cells of the Intestine

The multipotent intestinal stem cells are the only mitotic cells found within the midgut (Ohlstein and Spradling, 2006). There are estimated to be around 800 to 1000 ISC interspersed within an adult Drosophila midgut, specifically located near the basal membrane and adjoined with visceral muscle cells (Losick et al., 2011). The ISCs are responsible for the renewing of all the other cell types in the midgut every 1–2 weeks (Losick et al., 2011; Micchelli and Perrimon, 2006). This replenishment of the cells of the intestinal barrier is not only to balance natural turnover, but also for the regeneration

of the midgut after acute tissue damage or infection (Jiang and Edgar, 2011). In order to maintain the homeostasis, ISC division can be either symmetric or asymmetric, meaning that after division either both, none or only one daughter cell retains stem cell characteristics (Ohlstein and Spradling, 2007). In asymmetric division, the other daughter cell becomes an enteroendocrine cell or an enteroblast and subsequently differentiates, while in symmetric either both lose stemness or neither.

As proper functioning of the intestine and an adequate nutrient absorption is critical for any organism, it is crucial to understand how gut homeostasis is regulated and what signals initiate stem cell proliferation. There is evidence that ISC have regional differences regarding expression and proliferation, and may in part maintain the compartmentalization of the midgut through their identity (Jiang and Edgar, 2011; Marianes and Spradling, 2013; Miguel-Aliaga et al., 2018). While the ISC give rise to all of the cell types within the midgut, barring the VM which are of mesodermal origin instead of endodermal, their daughter cells seem to be epigenetically homogenous until their cell fate is determined by local signals, i.e. their differentiation is resolved by their environment (Losick et al., 2011). How this functional asymmetry of the daughter cells is obtained and regulated is complex and still under study.

The ISC express the marker genes *Delta* (Dl) and *Escargot* (Esg). Marker genes are selectively expressed genes that can be used to identify cell types.

2.3.1 Stem cell niche

The stem cell niche, or the conditions that promote stem cell survival and proliferation, is known to emerge from two main mechanisms: asymmetric signalling, e.g. hormonal balances, and adhesive interactions mainly with other stem cells and the VM under the basal membrane (Santos et al., 2018). In fruit fly the ISC niche is known poorly, but some regulatory signals have been revealed. Notch signalling has been found to be a major regulator of stem cell identity in the midgut (Micchelli and Perrimon, 2006; Ohlstein and Spradling, 2007). One coordinator of intestinal proliferation has been found to be metabolic status. For example, the stem cell adjacent visceral muscle cells have been found to locally regulate ISC through feeding-induced insulin signalling (O'Brien et al., 2011). The insulin-like peptide 3 that is expressed from these muscle cells compounds to systemic insulin signalling and can result to ISC activation (Choi et al., 2011).

2.3.2 Post-mitotic Cells

The ISC daughter cells can differentiate into several different cell types. The major types are the EEs and ECs, of which differentiation is dependent on Notch signalling pathway; high activity results in EC and low in EE (Ohlstein and Spradling, 2007). The dynamic of the differentiation is controlled, with around 10% becoming EEs and ~90% ECs (Micchelli and Perrimon, 2006).

Enteroblasts

The enteroblasts are the immature daughter cells of ISCs and the progenitor cells of the ECs. The EBs can be found apically to their mother cell, the ISC. EBs differentiate without mitosis and once differentiated it is terminal, i.e. there are no further differentiations or divisions (Ohlstein and Spradling, 2006). In addition to the Esg marker gene also expressed by ISC, the EBs also express Suppressor of Hairless (Su(H)), a downstream target of Notch. Due to the temporary nature of EBs, their presence is an indicator of current or recent stem cell activity.

Enterocytes

Enterocytes make up the vast majority of the intestinal cell population. They are a diverse group of polyploid cells and are responsible for the absorption of nutrients, maintaining regional acidity, and secretion of digestive enzymes (Hung et al., 2018; Miguel-Aliaga et al., 2018). In humans, ECs are known to be major consumers of glutamine, which is their primary source of metabolic fuel (Miller, 1999). The enterocytes can be divided into subtypes including copper cells, interstitial cells, and large flat cells, all of which are present in varying proportions in different regions of the midgut. Copper cells are gastric acid producing cells that modulate intestinal pH to enable digestion, and are consequently similar in function to gastric parietal cells in humans (Strand and Micchelli, 2011). Interstitial cells are characterised by apically reaching over copper cells, and have a postulated function in regulating copper cell behaviour (Strand and Micchelli, 2011). The precise function of large flat cells is yet to be described. The EB cell fate into interstitial cells and copper cells has been proposed to function through a mechanisms organised by the morphogen decapentaplegic (Dpp) that forms a gradient: low levels of Dpp lead to *defective proventriculus* (*dve*) activation and consequent differentiation to interstitial cell, while high levels of Dpp also induces *labial* (*lab*) gene expression, leading to differentiation into Dve^{+}/Lab^{+} copper cells, (Miguel-Aliaga et al., 2018).

One of the defining characteristics of the enterocytes is their ability to endoreplicate (Zielke et al., 2013). This means that while the ECs are post-mitotic, they can enter endocycles where their genome is replicated without mitosis and can consequently present programmed polyploidy. The ploidy-levels of the ECs are dependent on the nutritional status of the organism, and can reach at least 16N, i.e. 8 times larger than the diploid genome (Choi et al., 2011). The endoreplication is performed in order to increase cell and tissue size, and to increase the copy number and expression of cell type-relevant genes (Zielke et al., 2013). The copy number increase is of importance, as ECs are involved in the digestion and absorption of nutrients, and therefore need to produce high amounts of digestive enzymes and other digestion-related proteins.

Enteroendocrine cells

Enteroendocrine cells (EEs) are secretory cells that are a part of the endocrine signalling system. They produce a variety of hormones region-dependently (Ohlstein and Spradling, 2006). For example, a study found EEs to be able to express up to 4 peptide hormones region-specifically (Hung et al., 2018). In recent studies, it has been implicated that EEs are in fact differentiated from specific Prospero (Pros)-positive ISCs and not from EBs as had been thought previously (Zeng and Hou, 2015). Guo and Ohlstein proposed a model in which protein Pros is segregated to the daughter cell on the basal side during ISC mitosis, consequently committing the daughter cell to EE-fate (Guo and Ohlstein, 2015). The remaining ISC was also shown to require the adjacent daughter to have low-levels of Notch-signalling to retain multipotency. The EE have also been shown to have a role in forming the stem cell niche and ISC proliferation through nutrient-dependent signalling (Amcheslavsky et al., 2014). The homeodomain protein Prospero that also determines EE-fate is selectively expressed in EEs, and can be used as an EE marker (Micchelli and Perrimon, 2006).

Visceral muscle cells

The visceral muscle cells are smooth muscle cells that circle the midgut under the basal membrane. Unlike the other post-mitotic cell types of the midgut, the VM do not originate from the ISC. They are responsible for the gut peristalsis and therefore enable the movement of food and mixing with catabolic enzymes. The intestinal stem cell niche is also in part upheld by the VM; the VM cells secrete multiple signal molecules such as epidermal growth factor receptor (EGFR) ligand Vein (vn), JAK-STAT ligand Unpaired1 (Upd1), and Wingless (Wg) of the Wnt-family (Aghajanian et al.,

2016; Biteau and Jasper, 2011; Jiang and Edgar, 2011). This function is partially enabled by the EE, as they produce for example lipid-homeostasis regulating peptides called tachykinins that are also involved in the activation of expression of ISC-regulating insulin-like peptides by the VM (Amcheslavsky et al., 2014; Song et al., 2014).

2.4 Nutrition and the Midgut

The midgut is a nutrient-sensitive organ and is consequently highly responsive to changes in nutritional status (Lemaitre and Miguel-Aliaga, 2013). When in presence of abundant food, the ISC are signalled to increase proliferation rate, and as a result the midgut can grow in size to better process the food (O'Brien et al., 2011). A properly fed midgut has not only increased cell numbers and activity, but the cells have considerably larger volumes of cytoplasm, contributing to the growth in size (O'Brien et al., 2011). On the other hand, when food supply is low, the midgut reverts in size through reduced proliferation, natural turnover, and EC apoptosis in order to preserve resources (Choi et al., 2011; O'Brien et al., 2011). In other words, the midgut is a highly dynamic organ of which state fluctuates in response to environmental conditions and physiological cues. It is of note that when signalled to grow, the homeostatic balance of the midgut is interrupted, and therefore it can be presumed that these two functions have at least partly separate, yet integrated mechanisms of regulation.

In nature, *D. melanogaster* feed on fermented fruit at different stages of decomposition and their diet consists in large part of yeast fermenting the fruit (Lemaitre and Miguel-Aliaga, 2013; McKenzie and McKechnie, 1979). The cells within midgut express a diverse set of digestive enzymes. Most numerous of these enzymes are the proteinases with over 200 genes expressed in varying levels (Lemaitre and Miguel-Aliaga, 2013). Within the *Drosophila* genome, families of genes encoding for these different digestive enzymes are often arranged in clusters where each member has distinct expression patterns within the midgut (Buchon et al., 2013). The R0–R5 regions consequently have contrasting expression levels of different digestive enzymes, which is perhaps in part optimized by the gene family clustering. For example, the digestion of starch is performed sequentially: the middle regions express amylases for the breakdown of more complex carbohydrates and the posterior part processes simpler molecules (Buchon et al., 2013; Dutta et al., 2015). The posterior midgut has also

been described to have greater stem cell proliferation, which could be explained by the regions' major role in absorbing nutrients, i.e. the posterior midgut needs to respond to nutrient availability (Micchelli and Perrimon, 2006; Ohlstein and Spradling, 2006). The midgut also expresses 15 lysozymes that break down peptidoglycan in the bacterial walls, indicative of significant bacterial load in the diet of wild fruit flies (Kylsten et al., 1992).

Nutrient sensing and signalling

Nutritional status is known to greatly influence regulation of growth factors, which in turn can alter ISC activity and expression patterns (Buchon et al., 2013; Choi et al., 2011). One of the key pathways for accomplishing these changes is the insulin/IGF signalling pathway (InR signalling, Fig. 3)(O'Brien et al., 2011). For example, modulation of asymmetric and symmetric ISC division can be achieved by insulin-like peptide 3 (ILP3) signalling produced by the VM during rotations of feeding and starvation (O'Brien et al., 2011) However, the signalling by the insulin pathway is not clear-cut and requires modulation by other mechanisms; its activation can lead to either promoted or attenuated proliferation (Choi et al., 2011; Mattila et al., 2018). In a recent study by Mattila *et al.*, activation of hexosamine biosynthesis pathway (HBP) was found to regulate ISC proliferation and cause a

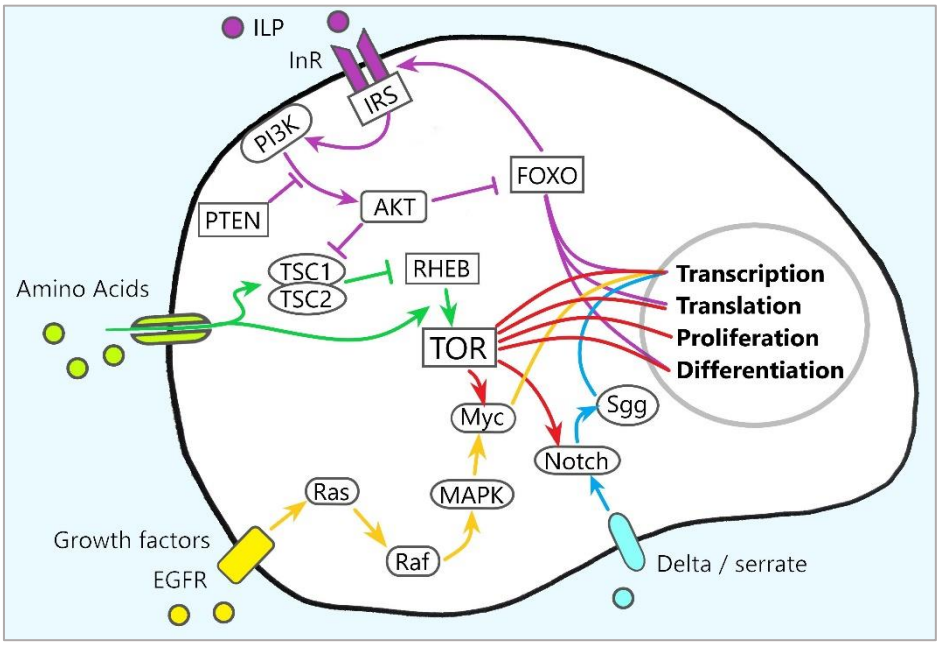

Fig. 3. Nutrient-responsive pathways in brief. *The regulation via nutrient metabolism is complex and multiple pathways are involved. Systemic growth factor signalling is intertwined with local nutrient-sensing in order to either activate or disable cell proliferation, differentiation, and protein production.*

Warburg effect–like metabolic switch, where cells prefer glycolysis over oxidative phosphorylation for energy production (Lee and Kim, 2016; Mattila et al., 2018). One mechanism for the variance of results obtained from activation of insulin was also revealed: HBP interacts with InR signalling. The stimulation of ISC proliferation through InR signalling was achieved when intrinsic HBP activity was low. The switch to Warburg effect-like status described by Mattila *et al*. subsequently allows greater activation of the TCA cycle and the production of necessary components such as fatty acids for proliferation. As glutamine is a precursor for HBP, it is of interest to study the effects of glutamine on stem cell activity.

The nutrient-dependent pathways do not only alter gene expression patterns and ISC proliferation but are also involved in cell fate determination. Evidence indicates that insulin signalling is required for ISC differentiation into both EEs and ECs (Choi et al., 2011; O'Brien et al., 2011) Additionally, the cytoplasmic and cellular levels of Delta (Dl), a Notch-ligand expressed by the ISC, have been found to be dependent on lipid-trafficking (Obniski et al., 2018). Dl is an activator of Notch, and consequently affects cell fates of ISC daughter cells. Moreover, insulin-like receptor signalling has been deemed required for EB fate determination into EC, but also for EC growth and endoreplication (Choi et al., 2011).

2.4.1 Glutamine

Glutamine (Gln) is a polar, water soluble and charge neutral amino acid that is an important source of energy for intestinal cells (Aledo, 2004; Miller, 1999). It is also the most abundant amino acid within human blood. Gln is exploited in multiple ways by cells, but its main roles are as an interorgan nitrogen shuttle due to its two amino groups, and as a carbon source for tricarboxylic acid cycle (TCA, also Krebs) (Fig. 4). Glutamine-derived intermediates from the TCA cycle are used in many important biosynthetic pathways to produce lipids, proteins, and nucleic acids (Yang et al., 2014). Consequently, Gln metabolism rate is greatly increased in rapidly proliferating cells and in damaged tissues (Aledo, 2004). In these situations, Gln can become limiting and as a result glutamine is regarded a conditionally essential amino acid in humans (Miller, 1999).

The breakdown of Gln is initiated with glutaminase-mediated removal of amide nitrogen, converting Gln to glutamate and releasing ammonia (Hensley et al., 2013). The amide group can also be transferred to sugars to create precursors for HBP in a step that is limited by Gln and facilitated by a

transaminase called glutamine fructose-6-phosphate amidotransferase (Gfat). Normally, in cells glucose is used as the primary source of carbon for the TCA cycle and is therefore the major source of cellular energy. However, in glucose-depleted conditions glutamate is used to transaminate ketoacids to form α-ketoglutarate (AKG) and ketogenic amino acids, respectively (Hensley et al., 2013; Yang et al., 2014). AKG is a TCA intermediate and can consequently be used in the cycle to produce for example NADH and ATP, and/or can be utilized in biosynthetic pathways. In proliferating cells, much of the different TCA cycle intermediates are used to produce components to allow cell cycle progression.

It has been widely reported that glutamine supplementation can have homeostatic or regenerative effects on intestinal health in patients on parenteral nutrition, i.e. feeding by passing the gastrointestinal tract (van der Hulst et al., 1993; Miller, 1999). For example, Gln supplementation preserved mucosal structure and prevented loss of deterioration in gut permeability, which is associated with bacterial infections and declined intestinal immunity (van der Hulst et al., 1993). Furthermore, glutamine deprivation has been found to cause quiescence in murine enteroid models (Moore et al., 2015). This effect could however be rescued by addition of Gln or alanyl-glutamine to diet. The once deaminated Gln, or glutamate, is also a precursor for glutathione, a cellular antioxidant which is also consumed for amino acid synthesis (Aledo, 2004; Hensley et al., 2013). Through glutathione, Gln can be employed as a buffer against oxidative stress.

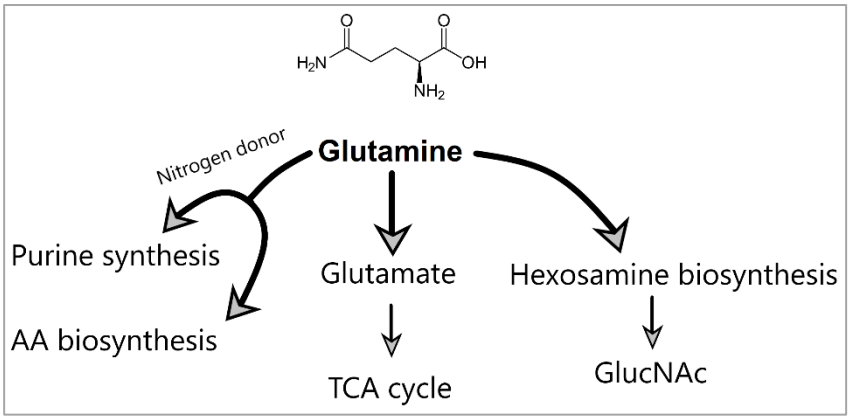

Fig. 4. Functions of glutamine. *Glutamine is used in multiple ways. Firstly, it contains two nitrogen atoms and is consequently used as a nitrogen donor for various reactions. Secondly, it is conditionally major source of carbon for TCA cycle resulting in energy generation and intermediates for biosynthetic pathways. Thirdly, glutamine is also a precursor for the initiation of hexosamine biosynthesis pathway.*

2.5 Outline

The regions within midgut are known to be functionally diverse yet remain for the large part uncharacterized. The regional cell populations are diverse and exact functionalities are obscure. Whether nutrient-dependent stem cell proliferation and differentiation are contingent upon their region-specific identities remains under study. As a plastic organ that responds to outside stimuli, the midgut and its stem cell-activating pathways can be studied by altering said stimuli. If the nutrient-dependent activation of stem cells is dependent on regional identities, then alteration of diet should lead to differing midgut-wide patterns in proliferation and differentiation. The exact effects of glutamine supplementation on the intestine are yet to be described, and consequently whether the reported beneficial effects of glutamine are due to direct activation of intestinal stem cells or due to some other downstream mechanism remains an outstanding question.

3. Aims of the Study

The aims of the study were two-fold: to study the effects of glutamine supplementation on adult *D. melanogaster* midgut and its intestinal stem cells, and to develop an applicable analysis method and protocol for whole-midgut microscopy images in order to effectively study the potentially ensuing cell population changes in the functionally different regions of the midgut.

4. Materials and Methods

As biological material is perishable and whole midgut imaging is time consuming, the experiments were done in batches and spread over a longer time period. The following protocol was performed multiple times to obtain enough material for the analysis. First, two strains were crossed, reared, and then dissected. The midguts were imaged with confocal microscopy and the image data was analysed with Imaris (Bitplane Inc, 2018). Afterwards, the data was exported from Imaris and analysed with a novel longitudinal analysis method. The work within the thesis was mainly concerning the

microscopy and data analysis, and consequently most of the dissected midguts were obtained by the courtesy of others.

4.1 Experimental Setup

Three nutritional sample groups were used in the study: starved, full holidic, and starved with glutamine supplementation. The full holidic medium is a nutritional, chemically defined diet designed for consistent experimental outcomes (Piper et al., 2014). The full recipes for all three media can be found in Appendix D. The starvation media contained no glutamine, while the full holidic and Gln-supplemented media contained 0.015% and 2% Gln, respectively.

4.1.1 D. Melanogaster Crosses

Two strains of *melanogaster* were crossed for the study in order to institute lineage tracing and to enable cell fate mapping. For the purpose of this study, lineage tracing can be described as a transgenic technique in which a heritable reporter gene is permanently activated in target cells, subsequently allowing the detection of the cells themselves and their progeny (Fig. 5) (Kretzschmar and Watt, 2012). The used method is an adaptation from the Gal4-UAS system (Brand and Perrimon, 1993; Duffy, 2002). The method utilizes a *S. cerevisiae*–originating transcription activator Gal4 that acts as a driver by binding to upstream activating sequences (UAS), and combines it with a flip-out system (Esg F/O) to promote the expression of green fluorescent protein (GFP) (Jiang et al., 2009; Micchelli and Perrimon, 2006; Smith et al., 2015). The activation of GFP expression in the progeny is achieved with a recombinase flippase (FLP).

Genetic Basis and Function

The crossbreeding was done by mating a strain containing Esg Flip-out (esg F/O) system with a strain with enteroblast marker and a balancer chromosome. Both of the strains thus had one of the following genetic constructs:

1) **Esg F/O***: w; esg-gal4 tub-gal80^{ts}* UAS-*GFP;* UAS-*Flp Act*>CD2>*Gal4*
2) **EB marker**: *Su(H)-LacZ*; TM6B

The first genotype contains a repressible cell marker for GFP-labelling ISCs and for activating Gal4 transcription factor (TF) expression in daughter cells. The Gal4 is initially only expressed in ISCs and EBs as the *Esg*–gene is selectively expressed in these cells. The UAS-*Flp* transgene is conditionally activated by the expression of Gal4. The α-*Tubulin* (*Tub*)-*Gal80* construct encodes for a heat-sensitive mutant of Gal80, which is a negative regulator of Gal4 (Lee and Luo, 1999). Gal80 inhibits Gal4 from transcriptionally activating *GFP* and *Flp* through dimerization, which results in the masking of activation domain of Gal4. When transferred to a higher temperature of 29 °C, Gal80 becomes deactivated and dissociates from Gal4. Subsequently, the UAS-Flp construct will be activated, and the heat-activated flippase recombinase excises the CD2 cassette by recombining flippase recognition targets (FRT) flanking the CD2, subsequently allowing the expression of Gal4 downstream of *Actin* (Act) promoter (Golic and Lindquist, 1989). As this recombinant sequence is under the *Act*s promoter and is expressed globally, also the differentiated daughter EEs and ECs will produce Gal4 and activate the transcription of the UAS-*GFP* transgene. The second construct has the *Su(H)-LacZ* transgene that is selectively expressed in enteroblasts and produces β-galactosidase that can be visualised by immunofluorescent staining. Considering the heat activation of the recombinase, an experiment can be set up so that the CD2 cassette is removed only once desired, i.e. onwards from the time point the lineage tracing is required.

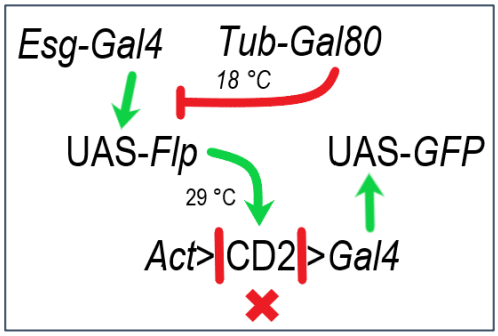

Fig. 5. UAS-Gal4-GFP lineage labelling. Gal4 *is downstream of* Escargot *and is expressed in* progenitors. *A Gal4-binding UAS-enhancer activates the expression of Flp when in higher temperature of 29 °C. When activated, Flp excises the CD2 cassette. Under promoter of* Act, *Gal4 can be transcribed in all non-progenitor daughter cells. In* Esg*-active cells, GFP can be immediately produced if Gal4 is not inhibited by Gal80, i.e. when at higher temperature.*

In addition to these labelling constructs, the crossbreeds also have TM6B balancer chromosome (Miller et al., 2016; Pina and Pignoni, 2012). Balancer chromosomes are phenotype causing modified chromosomes that can be used to screen for heterozygosity. When present in the genome, the TM6B balancer triggers a tubby phenotype presenting itself as a shortened and rounded body shape in the larvae and pupae. Moreover, the balancer contains multiple inversions that in case of recombination

lead to non-viability of the offspring. Owing to these characteristics of the balancer chromosome, selection of progeny that have the gene constructs can be visually.

4.1.2 Rearing and Feeding

For the crossbreeding, the strains were grown on standard growth media (Appendix D) and sexed by morphological differences, i.e. the males have dark posterior abdomen while for females the abdomen is more elongated. To enhance egg laying, the flies were provided with dried yeast. The flies were kept at 18 °C and on standard growth medium until the beginning of the experiment in order to inhibit Flp activity. After several days the flies were discarded, and pupae were collected selectively (Fig. 6). All pupae with the balancer chromosome, i.e. presenting the tubby-phenotype, were discarded. All animals were collected into vials containing starvation media. This was to establish a baseline nutritional status for studying the effects of transferring to a new, altered nutrient regimen. Accordingly, the starvation sample group functioned as a control group for the nutritional effects. The purpose of the holidic group was to have a reference for well-fed midguts in order to determine glutamine-specific effects from effects due to improved calorie intake. After eclosion, mated flies were collected and transferred to starvation, holidic, or Gln media, 15 females and 7–9 males each. The flies were kept at 29 °C for 7 days to activate the lineage labelling and to accumulate nutritional effects.

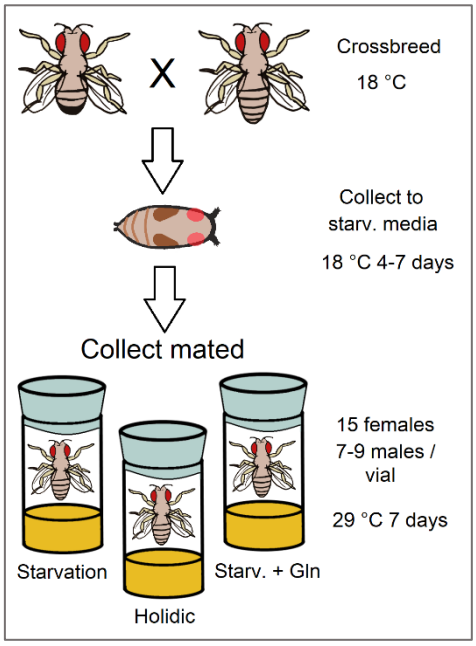

Fig. 6. Experimental setup. *Two strains of* D. melanogaster *were crossbred and kept at 18 °C. Resulting pupae were then collected to starvation media and grown for less than a week. Non-virgin flies were then collected to the three experiment media and grown for a week at 29 °C to activate lineage labelling.*

4.1.3 Dissection and Mounting

After 7 days, the midguts were prepared for mounting onto spacer microscope slides. Flies were first collected into phosphate buffered saline (PBS) for dissection. The dissection was performed on a microscope slide with precision forceps under a microscope. First, a fly's head was cut off to sever the gastro-intestinal tract. The posterior abdomen was then grasped with forceps by the anal plate, followed by careful pulling out of the intestine. Any debris was removed and malpighian tubules were

cut off. The midguts were then straightened and arranged parallel to each other. After, fixing of the midguts onto the slides was performed with either 4% or 8% paraformaldehyde in PBS (PFA) for one hour. The midguts were then rinsed twice with PBS solution with 0.1 % triton (PBT). The midguts were then incubated for 1 hour in blocking buffer consisting of PBT with 1% bovine serum albumin (BSA) in order to block non-specific binding sites for antibody treatment. Incubation with antibodies was performed overnight at 4 °C. Two primary antibodies were used: mouse anti-Prospero 1:1000 and rabbit anti-β-galactosidase 1:400 in blocking buffer. After overnight incubation at 4 °C, the tissue was washed four times with PBT. Subsequently, the midguts were incubated with the secondary antibodies containing the fluorescent dyes: anti-mouse Alexa^{647} and anti-rabbit Alexa^{568}, both 1:1000 in blocking buffer. After, the midguts were washed four times with PBT. The midguts were then mounted in circa 25 µl of Vectashield mounting medium with DAPI (1.5µg/ml). After a short incubation of approximately 15 minutes the midguts were ready for microscopy. The prepared microscope slides were stored in a cold room at 4 °C.

4.2 Microscopy

A whole-midgut imaging was performed using Aurox Clarity spinning disc confocal microscope. Only one side of the midguts was imaged, i.e. the epithelial wall nearest to the microscope slide. The midgut has not been shown to contain variation along its circumference and consequently studying only one side of the wall has been deemed a sufficient cross section of the whole.

4.2.1 Fluorescent Stains

Overall, the midguts were stained with three fluorescent dyes, excluding the GFP produced by the lineage labelled cells. These were the DAPI-stain included in the Vectashield mounting medium, and the Alexa^{647} and Alexa^{568} contained in the secondary antibodies. DAPI stains the nuclei of the cells by binding to A/T -rich regions and when excited emits light with maximum peak at a wavelength of 358 nm. Alexa^{647}, Alexa^{568} and GFP emit light at a maximum at 665, 603, and 509 nm, respectively. Consequently, the dyes could be multiplexed and each of the emissions was captured through different filters (Table 1).

Table 1. Description microscopy channels and filter cubes. *Four colour channels were used in total. The used microscopy system used white-light source and the filter cubes are used to pass only excitatory wavelengths toward the sample and emission wavelengths towards the detector. The filter cubes were produced by Aurox for the Clarity system.*

Fluorophore	Target	Filter Cube	Product no.	Specifications (nm)
DAPI	Nuclei	DAPI-LED	0401	ex 392/23, em 447/60
GFP	Progenitors, progeny	GFP-LED	0406	ex 466/40, em 525/45
Alexa^{568}	EE (Pros)	DsRed-LED	0403	ex 554/23, em 609/54
Alexa^{647}	EC (Su(H))	Cy5-LED	0408	ex 635/18, em 680/42

4.2.2 Aurox Clarity Spinning Disc Confocal

The Clarity system is a laser free spinning disc confocal microscope (SDCM) that utilizes structured illumination microscopy (SIM). SDCM uses spinning discs with pinholes to project multiple beams across the sample to gain faster scanning times than in traditional laser-scanning confocal microscopes (Jonkman and Brown, 2015). While SDCM has relatively lower resolution, for the purpose of quantification of cellular populations, an increase in subcellular resolution would have been of limited use. Additionally, the faster imaging time was crucial as several dozen image stacks are needed to capture the whole of the midgut (Fig. 7).

SIM is a method where the excitation light and the disc is used to produce an interference pattern to create optical sectioning (Langhorst et al., 2009). This subsequently allows for differentiation of out-of-focus and in-focus light, and calculation of additional information from the sample that results in a clearer picture. In simple terms, by capturing multiple pictures the differing patterns can be subtracted from each other to obtain a sharper image (Jonkman and Brown, 2015).

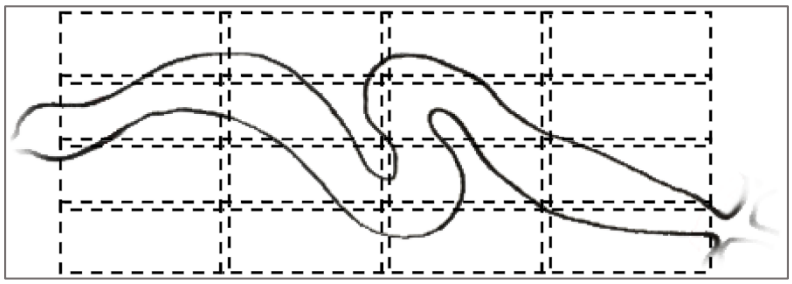

Fig. 7. Aurox whole-midgut imaging. *Imaging of whole midguts is time consuming as a large grid of images is needed. For this, the swiftness of SDCM is helpful.*

The Clarity system excites the fluorophores in the sample with light from a widefield white-light source (Leica EL6000) that is passed through colour channel–dependent filter cubes to limit passed wavelengths into the excitatory spectrum. After passing the spinning discs pinholes, the light intensity is low enough to not cause any significant photobleaching, consequently allowing continued imaging (Jonkman and Brown, 2015). The emitted fluorescence again passes the disc and is let through wavelength respective filter cube and is then imaged by a scientific complementary metal-oxide-semiconductor (sCMOS) image sensor (Hamamatsu Orca-Flash 4.0 V2). The images were pictured at either 20x (Leica HC PL APO CS) or 63x (Leica HCX APO Corr (glycerol) CS) magnification with numerical apertures (NA) of 0.7 and 1.30, respectively. NA indicates the resolving power of the objective, i.e. how near two features can be in order to be distinct. The final resolution is dependent on the light source's wavelength and the refractive index of used medium in addition to the NA.

4.3 Image Analysis

The microscopy images were analysed for changes in cell population. The exploratory analysis itself was performed in Imaris v9.2.1, a microscopy image analysis software (Bitplane Inc, 2018). It facilitates an interactive, real time visualization of 3D and 4D microscopy image datasets, consequently enabling intuitive assessment of experiments. The in-built tools and extensions offer various possibilities for extracting data of interest in an easily exportable form. Main functionalities that were used in the analysis included Spot, Surface, and Filament –object creation, signal filtering, and several in-built and extension functions.

4.3.1 Image Pre-processing

Several steps were taken before the proper analysis. The midgut images from Aurox come in multiple stacks, or a multistack, that were first stitched together using Imaris Stitcher v9.2.1. One of these multistacks can include several hundred image slices that each contain data from one microscopy channel. In the XY-plane, the multistack is divided into stacks that each contain the Z-dimensional data of one location, i.e. up and down from the microscope stage. The metadata of the multistack holds information on how the individual slices and stacks are spatially related, that can be used to place and stitch the multistack into a 3D image (Fig. 8).

Due to the nature of the imaging system, several steps of signal processing were first performed to the 3D images. The multistacks contain plenty of image data outside the midgut, which had to be filtered out to not interfere with the data of interest. Although the samples were washed during the mounting, the slides still included an abundance of debris, shed cells, and larger cell aggregations. Additionally, on some channels the light noise was at times enough to warrant filtering. The filtering was executed by creating Imaris Surface -objects and subsequently setting all outside values to zero (Fig. 9A). The operation was performed twice: first with hand–drawn surface borders to exclude any larger signal causing aggregations, and then by automatic creation that approximates the midgut walls

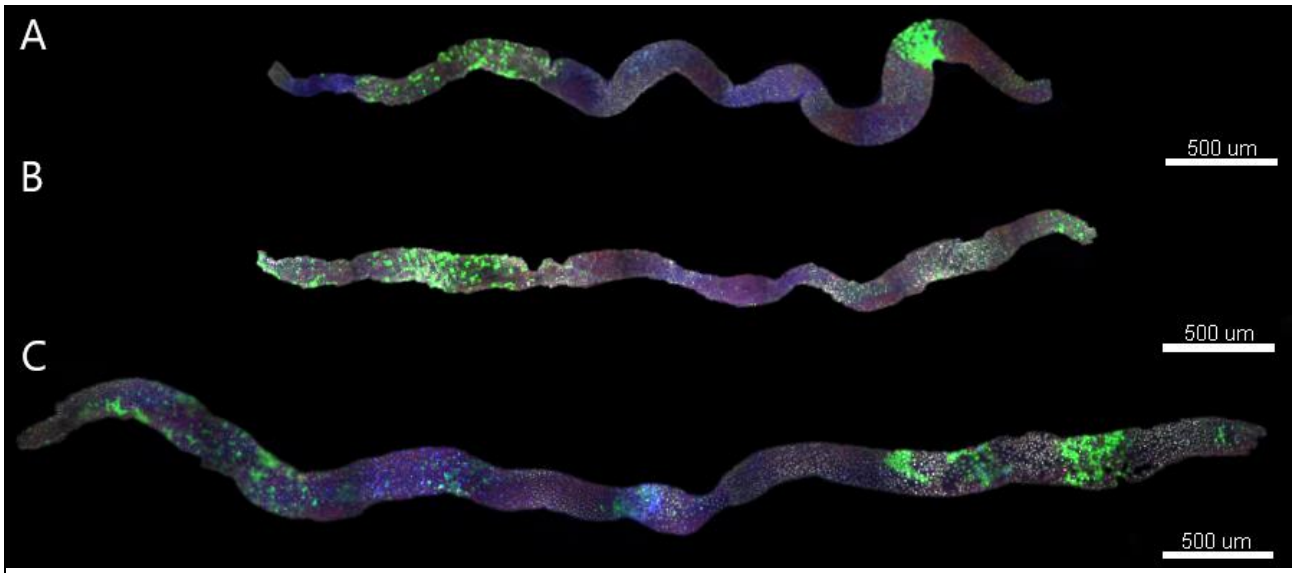

Fig. 8. Stitched Aurox-microscopy images. *Composite picture of three midgut multistacks.* ***A)*** *Glutamine supplemented midguts tend to get some characteristics alike to well-fed, e.g. the posterior part can seem more pronounced.* ***B)*** *A starved midgut is small relative to well-fed midguts.* ***C)*** *Midguts that were kept on a holidic diet have great increases in length and thickness.* ***Colours:*** *lineage labelled cells shown in green, EBs are blue, EEs are red, and DAPI is shown as shades of grey/white.*

more efficiently. Once the detrimental signals were removed, other object creation algorithms could be used more powerfully.

4.3.2 Spot -object Creation

The Spot -objects were used to determine cell coordinates from the signal (Fig. 9B–D), and were created for each used channel: GFP, Pros, Su(H), and DAPI. The algorithm uses Laplace operator of a gaussian filter to detect the spots, i.e. cells are found by detecting divergence in signal intensities between regions of the image (Kong et al., 2013) The algorithm determines the cells from the background based on several criteria. Foremost, it considers the XY diameter of the signal feature, but can also be set to account for the ellipticity of the feature. The sizes of the features are also dependent on minimum and maximum cut-off points of signal intensity, which was also used to curtail noisy features from creating ambiguous Spots -objects. The Imaris' automatic creation algorithm was used with varying parameters depending on microscopy channel (Appendix E). For

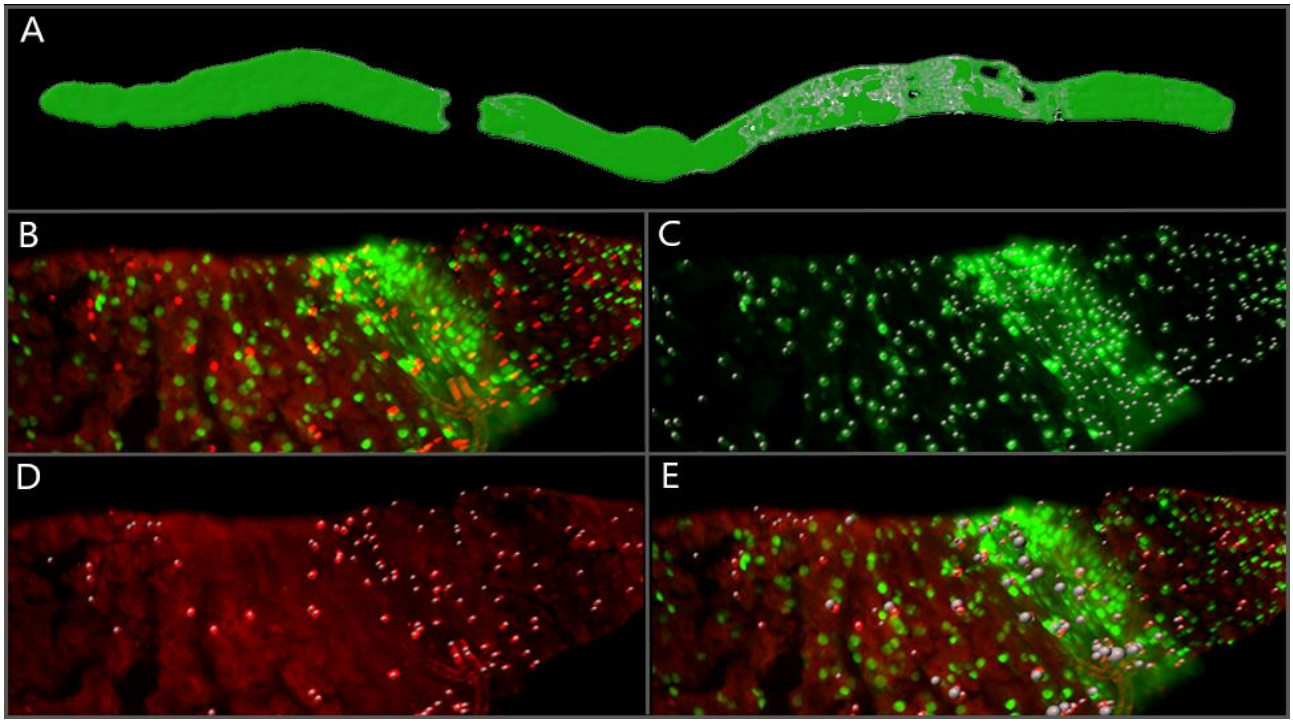

Fig. 9. The Imaris Surface and Spot -object creation and detection of cell locations and determination of nucleus area. A) *secondary Surface used for filtering irrelevant signal intensities outside the midgut.* ***B)*** *a combined channel of GFP and Prospero.* ***C)*** *GFP-channel with Spots -objects denoting locations of ISC and their daughter cells.* ***D)*** *Prospero-channel with Spots marking the locations of EE cells.* ***E)*** *Pros+GFP -channel with co-localised volumetric Spots, or EE cells of known volume and that have originated during the experiment.*

example, the Prospero–antibody complex tended to aggregate, forming small signal features reminiscent of cells, consequently demanding stricter control of parameters in the lower end.

Besides the location of the cells, the distance between nuclei was also of interest as newly created cells are closer to their mother cells. To determine the distance to nearest nucleus for each cell, Imaris extension "Spots to Spots Closest Distance" was used. Of additional interest was also the size of the nuclei, as it is a sign of endoreplication. Imaris includes a seeded region-growing method for determination of areas of Spots -objects which was used for the determination of nuclear areas from DAPI-channel voxel intensities (Adams and Bischof, 1994; Fan et al., 2005). Seeded region-growing is an image segmentation method, in which the seed inputs function as initial intensity values to which nearby voxels are compared to for similarity. Each voxel is compared to nearby seed regions' mean intensities and is assigned to the most similar, therefore increasing the volume and area of the region. As the Spots -objects functioned as seeds, their initial creation parameters were of essence in the establishment of regions that correctly approximate the nucleus of the cell from the DAPI-channel intensities.

For the detection of co-localising signals, Spots -objects from one channel were filtered by intensity from another (Fig. 9E). The cut-off intensity was determined by eye for each sample and channel due to differing levels of noise. The co-localisation channel objects were created for GFP+Pros and GFP+Su(H) in order to detect newly created and differentiated EE and EC cells, respectively.

4.3.3 Anterior, Posterior and R3

Once all Spots -objects were created, Imaris' FilamentTracer tool was used to mark each of the anterior, posterior and middle regions. The FilamentTracer allows for manual drawing of lines that can be used for a variety of functions. The Imaris extension "Spots Close to Filaments" was then used to find each cell belonging to the region (Fig. 10). The extension finds each Spots -object within designated distance from the Filament. Due to irregularity in the widths of midguts, the used distance varied between 100–250 µm. The midgut

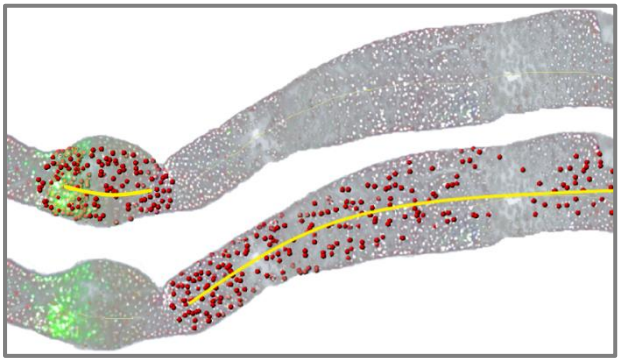

Fig. 10. The Imaris Filament -object creation and detection of anterior/middle/posterior cell populations. *Filament and Prospero Spot -objects in a midgut fed with full holidic diet. Upper: R3–region. Lower: posterior region.*

region assignment was performed to Spots -objects procured from each channel, including the co-localisation channels.

4.3.4 Data Collection

For the exploratory study, only cell numbers were collected, i.e. overall midgut cell populations and populations within the regions specified by the Filaments. Imaris stores a plethora of information from the created objects that can be readily exported as csv-files. All the different created Imaris objects within a sample have specific identifiers, or ID's, that are used to associate data between csv-files. The rest of the obtained data was analysed with a novel longitudinal analysis method.

4.4 Longitudinal Analysis of the Midgut

The exploratory image analysis data via Imaris highlighted the positional variation that exists within the midgut between different sample groups. The anterior–middle–posterior -division used, while sensitive enough to perceive some differences, had inadequate resolution to postulate on the underlying biological causes of the variation. These results functioned as an incentive to create a novel, incremental whole-midgut analysis method in the spirit of sliding window analyses (Fig. 11). The analysis method utilizes DAPI-channel nucleus positions found by Imaris' Spot -object algorithm in order to create a running median that approximates the midgut along its whole length on an XY -image plane. The running median then functions as a vector onto which signal locations are projected by minimum distance estimation, consequently allowing analysis of all used image channels of the data with reduced dimensionality, i.e. the signal location can be described with only one coordinate dependent on its position along the midgut in the antero-posterior axis.

4.4.1 Preface

The created Longitudinal Analysis of Midgut (LAM) functions as an extension to the Imaris analyses. In other words, all steps in the Imaris analyses are required, except for the anterior/middle/posterior filament creation. In addition to the Spot creation in Imaris, two further Measurement Point -objects (MP) were generated to mark both the R3 region and the boundary between R4 and R5 regions in order to centre the separate samples for appropriate comparison, and to account for length differences, respectively. The R4/R5 -boundary was identified visually, as the boundary typically has smaller

cells and a higher cell density than the surrounding regions, which can be used as a defining characteristic. However, the change is not always evident, and hence the measurement point was created for only a subset of samples.

The length of the midgut is variable and dependent on the nutrient content of the fruit fly's diet, and consequently the lengths of the guts were normalized to a percentage from cardia to midgut–hindgut junction, as has been done in a previous study (Buchon et al., 2013). On a full holidic diet, growth in length can be attributed to enlargement of cytoplasm and increased cell numbers. Because of the enlargement, the method was designed to have the capacity to compare both total numbers and fractions of different cell types between the sample groups. As cell density is varied due to the size of the cytoplasm, the effects of nutritional alteration could perhaps in some cases be better comprehended via fractional variation, i.e. changes in cell numbers divided by total number of detected nuclei. Additionally, the fractionation guarantees some protection against non-optimal binning of projections due to a misplaced section of the vector, i.e. when the median does not closely follow the centreline of the midgut. However, for the purpose of the thesis LAM utilizes only total cell counts. This has the advantage of revealing the true changes of cell population size between the different sample groups.

4.4.2 Method, Step-by-Step

The script first analyses the samples separately and then organizes samples into groups for analysis between sample groups. The XY-coordinate locations for Spot -objects in the DAPI-channel from Imaris were first used to create the vector. The Z-coordinates of the objects were not used for the analysis, as they would not influence the projection onto the vector: the nearest point on the XY-dimensional vector is independent of the cell location on the Z-axis. Furthermore, the total Z-stacks in the microscopy images did not exceed more than 2–3 cell widths, as only one side of the tubular intestinal wall was under scrutiny, i.e. the epithelium nearest to the microscope slide. The analysis method has the flexibility to use different bin sizes for the creation of the running median and the projection in order to allow for analysis of specific regions of the midgut instead of all regions, but for the purpose of the thesis, whole midguts were used. A total of 35 bins were used for the creation of the running median and 100 bins for the projection onto the vector. The binning in the vector creation must was carefully selected, as it affects the efficacy of how well the median approximates the shape of the midgut under study. If too many bins are used, the median may fluctuate due to

differences in cell density, and if too few are used, the median may skip over minor grooves in the shape of the midgut.

The script was designed to assume that each directory at its file location contains the data files for one sample. The sample directory and file names contain information that the script utilizes to group and sort the large amount of data used in the analysis. The script first loops through all directories, one sample at a time, and performs the following operations:

1) Reading of the DAPI–coordinate file
2) Creation of the vector from the locations
3) Collection of coordinate data of all other channels found in the sample directory
4) Collection of additional data if the sample directory contains the related files. This includes cell area, microscopy channel intensities, and distance to nearest nucleus.
5) Projection of signal coordinates on all channels onto the vector, including DAPI
6) Collection of the R3 and R4/5 coordinates and their projection
7) Storage of projection data into channel-specific Pandas DataFrame –objects (DF), one column for each sample (McKinney, 2010)

After data from all samples have been collected and grouped, the following operations are performed:

1) The centring of the samples by their respective R3 MPs
2) Subjection to plotting and statistical testing

Vector creation

From anterior to posterior, the first and last cell of the midgut are first found by minimal and maximal X-axis locations. The space between these points is then divided into equally large, predetermined number of bins. For each of these bins, the largest and the smallest y-axis value is found from the cell coordinates that fall into the bin. The median Y-axis -coordinate between these cells is then assumed to be the middle point of the width of the midgut. In case of an empty bin, e.g. when the midgut has a breakage with no cells, the median of the earlier bin is re-used. As the X-axis locations of each bin is known, the Y-median coordinates can then be expressed as points on the image. The X-locations

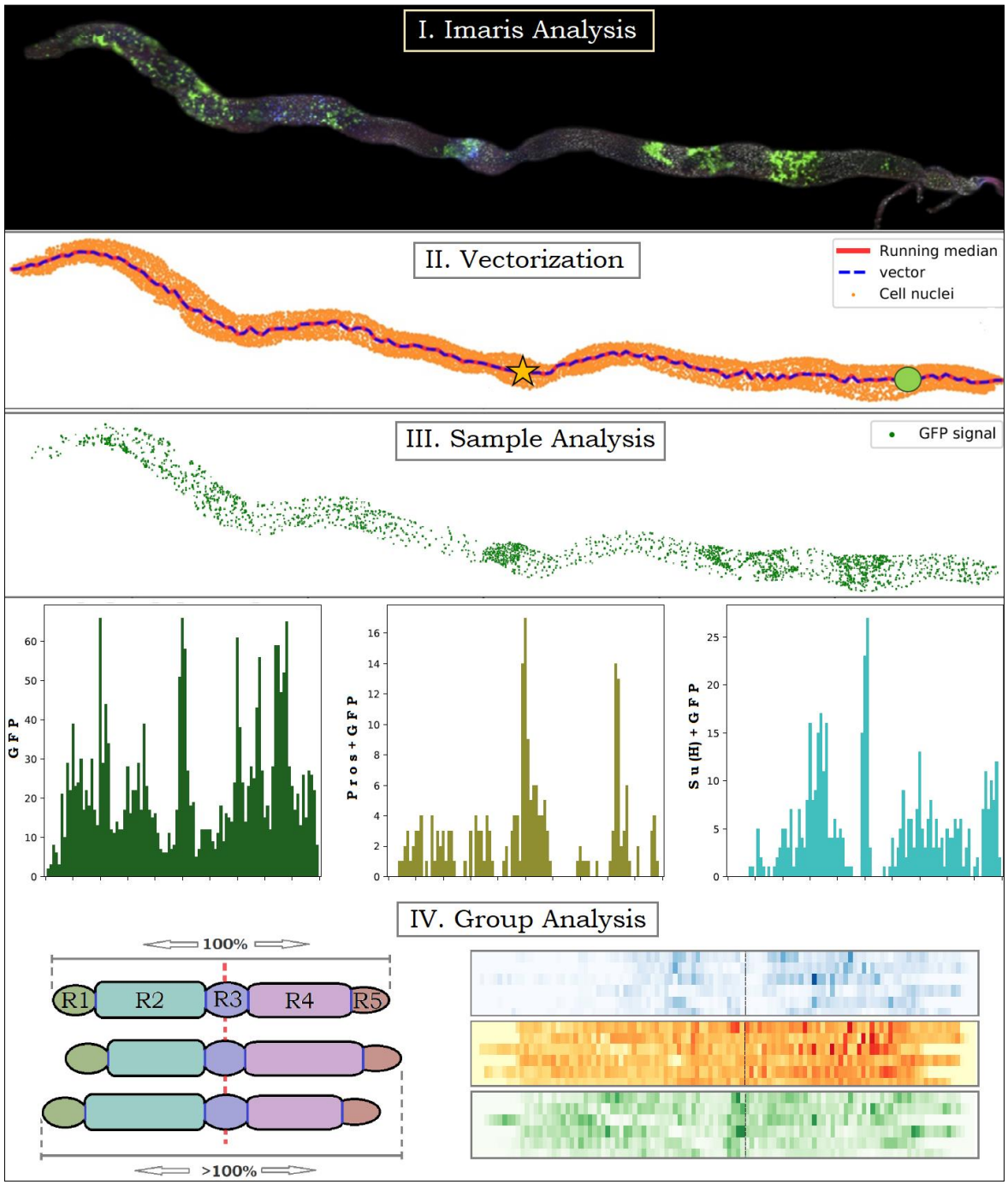

Fig. 11. Longitudinal analysis in brief. I) *After imaging, all cell locations are found on their respective channels using Imaris.* ***II)*** *Cell nuclei positions are used to create a running median to approximate the midgut. Star: location of R3. Circle: location of R4–5 -boundary.* ***III)*** *Signal locations and co-locations of the wanted channels are then separately projected onto the vector. The projections can then be plotted on the longitudinal axis.* ***IV)*** *Once all samples have been analyzed, they are subjected to group analysis. The measuring point in the R3 -region is also projected and is used to center the midguts for location-wise comparison (red line). One midgut has a length of 100%, but due to variation in proportions, the sample groups exceed the length. After, the groups can be plotted and examined with statistical tests.*

of the bins and their respective Y–medians are then transformed into Point–objects and used to create a LineString -object with the *Shapely* package (Gillies *et al.*, 2007). The transformation into Point -objects is required for the LineString–creation function. LineString -objects themselves are collections of coordinates that form continuous lines and have several advantageous attributes: the coordinates of points along the line can be obtained without difficulty, the lengths of the lines can be determined effortlessly, and discrete objects can easily be projected on to the nearest coordinate belonging to the line. Consequently, the Shapely package provides a powerful tool for vectorizing the running median for the subsequent analyses.

Signal coordinate projection

The signal XY-coordinates of a channel are first transformed into Shapely MultiPoint -object, which is a collection of Point -objects, and are subsequently projected onto the vector. The projection itself is done with linear referencing methods found within the Shapely package: the functions project() and interpolate(). The project() -function returns the distance to the point along the vector that is nearest to the signal coordinate and the interpolate() gives the coordinate of the point at the specified distance along the vector. These coordinate points are then ordered into their respective bins along the vector using *Numpy*'s digitize() -function (van der Walt et al., 2011). The cell numbers in each bin are then counted and formed into an array of which index indicates the location of the bin along the midgut. The projection of the R3 and R4/5 is done similarly, but their data files only contain one coordinate point: the location of the Imaris Measurement Point -object on the microscopy image.

Additional data

The Imaris data files contain numbered cell ID's for each cell of a sample which can be used to link data in separate files. Consequently, any cell-specific data from Imaris can be used in the analysis. For the purpose of this thesis, area of DAPI-channel Spot -objects and minimum distance between nuclei were used. As all this data is denoted by the cell ID, once a position has been projected, the additional data related to that position are also marked to belong into the corresponding bin.

Centring and follow-up operations

After the data collection, the samples are grouped and centred with the R3–MP. For this, a zero–filled DF of larger length than an individual sample is created for each channel. For each of the samples,

the bin of the R3 is found, and the sample's cell count array is inserted into the DF respective to the bin, i.e. all R3–MPs are located at the same DF index position. This is necessary as the DFs have fixed dimensions, and because a sample may have different number of bins in the anterior and posterior ends due to variable proportions of the midgut. As a result, all channel data is stored into a DF with zeros in the head and tail ends of the samples. In the subsequent operations, the left-over zeros are transformed into Numpy NaN -objects that do not affect the respective calculations or are alternatively dropped altogether. Afterwards, the data is passed on to plotting and plot-wise functions, and for statistical testing using *Mann-Whitney-Wilcoxon U test* (MWW). All these functionalities are included within the base code of the method.

4.5 Statistical Testing

The statistical testing between sample groups during LAM–method is performed to all bins of a channel sequentially with Mann-Whitney-Wilcoxon U test with false discovery rate (FDR) and continuity correction (Benjamini and Hochberg, 1995; Mann and Whitney, 1947). For MWW, LAM utilizes S*cipy.stats* –package's mannwhitneyu() -function, which includes continuity correction as a parameter (Jones et al.). The FDR correction is performed with *mne.stats* -package's fdr_correction() -function (Gramfort, 2013; Gramfort et al., 2014)

Mann-Whitney-Wilcoxon U test

Once the sample group–DFs are passed on to the MWW -functionality, each bin of the control group in each channel is consecutively compared to the respective bin on other sample groups based on index-location on the DF. In other words, the signal counts at a specific longitudinal location from all the samples belonging to the control group are compared to the signal counts at the corresponding location in the other sample groups. The locations tend to have variance and are not normally distributed (see Appendix B), and as a result a nonparametric test is required. Additionally, the data is discrete and not continuous, and therefore requires the continuity correction. The MWW is often described to compare medians of the two groups, but in reality a more accurate description would be that it tests for significant differences in the groups' distributions (McElduff et al., 2010). However, MWW can be described to measure whether the other group is stochastically greater than the other.

Considering two populations X and Y, MWW's hypotheses are as follows:

H_0: The populations are equal, or $P(X > Y) = P(Y > X)$

H_1: The populations are not equal, or $P(X > Y) \neq P(Y > X)$

Consequently, MWW tests whether it is equally likely that a randomly selected observation from one group will be greater or less than from another group. The test first pools and ranks all observations in both populations based on their values, i.e. the smallest value is ranked as 1 and the highest value is ranked as N, i.e. the combined number of observations in both populations. In case of tied values, they are ranked as the midpoint of unadjusted rank: if we have four values of 5 which would be ranked 3, 4, 5, and 6, all their ranks would be $\sum_{i=3}^{6} {}^{i}/_{4} = 4.5$. The ranks are then used to calculate U statistics for both populations followingly:

$$U_1 = R_1 - \frac{n_1(n_1 + 1)}{2} \tag{1}$$

$$U_2 = R_2 - \frac{n_2(n_2 + 1)}{2} \tag{2}$$

where *n* is the size of the population and *R* is the sum of the ranks within that particular population. Summing equations (1) and (2), and realizing that the total population $N = n_1 + n_2$ and the sum of all ranks $R_1 + R_2 = N(N + 1)/2$, it can be derived that:

$$U_1 + U_2 = R_1 + R_2 - \frac{n_1(n_1 + 1)}{2} - \frac{n_2(n_2 + 1)}{2}$$

$$2(U_1 + U_2) = (n_1 + n_2)(n_1 + n_2 + 1) - n_1(n_1 + 1) - n_2(n_2 + 1)$$

$$U_1 + U_2 = n_1 n_2 \tag{3}$$

From equation (3) can be seen that the U statistics of the compared sample groups are dependent, and that when e.g. U_1 nears $n_1 n_2$ then U_2 must near zero. The total U score of a population can also be described as the sum of the U statistic of each of its observations, with each observations U statistic being the number of the other populations observations it is greater or less than. The combinatorial

selections from the full set of observations can be used to define the populations' asymptotic distribution, which should be approximately normal under the condition of large enough population, which is approximately 20. However, as normal distribution is continuous and the U statistic is binomial, a continuity correction is required. This is done by adding or subtracting 0.5 from the U–value based on certain criteria. Following this, a z-score can be calculated:

$$z = \frac{U - m_U}{\sigma_U} \tag{4}$$

where σ_U is the standard deviation of U and m_U is the mean of U. The respective *p*-value is straightforwardly obtained from a standard normal table using the z-scores obtained from eq. (4). In the case of LAM, the mannwhitneyu() -function calculates the *p*-value for each test.

FDR adjustment

The *p*-values are subsequently subjected to Benjamini–Hochberg FDR procedure to account for type I errors (Benjamini and Hochberg, 1995). Type I errors are false rejections of null hypothesis, which are likely to happen when performing multiple significance testing. If ranking *p*-values of *m* total hypotheses in ascending order as $P_{(1)} \ldots P_{(m)}$, then the FDR correction functions by finding largest *i* that satisfies

$$P_{(i)} \leq \frac{i}{m}\alpha;$$

where α is a given error rate. For all *p*-values smaller than $P_{(i)}$, the null hypothesis is then rejected, i.e. declare discovery. For LAM, an α of 0.05 was used.

5. Results

For the exploratory analysis the sample sizes were 27, 26, and 17 midguts for holidic, starved, and starved+Gln sample groups, respectively. For LAM, due to restrictions on vector creation a smaller set of samples from these were used (Table 2). Furthermore, the applied Su(H) and Pros targeting stains at times lead to overall noise or cell-like aggregations that lead to confounding signals. Consequently, depending on batch and the sample some of the channels were dropped from both analyses. The whiskers for the following boxplots were defined by a cut-off point of 1.5 times the interquartile range (IQR), where IQR means the median of the upper quartile minus the median of the lower quartile. Therefore, all data points past these were considered outliers.

Table 2. Sample sizes for LAM. *DAPI-channel denotes the total sample size due to it being the vector creation channel. On other channels, some samples were excluded from analysis due to excess noise.*

CHANNEL	STARVED+GLN	HOLIDIC	STARVED
DAPI	14	19	15
GFP	14	19	15
SU(H)+GFP	14	18	15
SU(H)	13	19	15
PROS+GFP	9	19	12
PROS	9	19	12

5.1 Changes in Total Cell Numbers and Midgut Size

Both holidic and Gln sample groups had significant increases in total cell numbers (Fig. 12A). The increase is most prominent in holidic diet with 6385±936 nuclei versus 5213±1072 in starved. Glutamine supplementation increased the total nuclei, albeit with a great variation, to 6078±1313 (p=0.015). Only minor increases in size of the midgut were detected with glutamine supplementation; an area of 1.45±0.22 mm^2 with Gln versus 1.33±0.16 mm^2 for starved. In contrast, the well-fed midguts increased greatly in area to 2.42±0.27 mm^2. The area here denotes the area of the Imaris Surface-object that was used for the final filtering of the microscopy images. Consequently, the values approximate the surface areas of the midgut cross-sections, i.e. the epithelial walls against the microscope slide. The acquired differences in areas can in large part be explained by increased volume of cytoplasm in the holidic group, as shown by the microscopy image comparison and the average

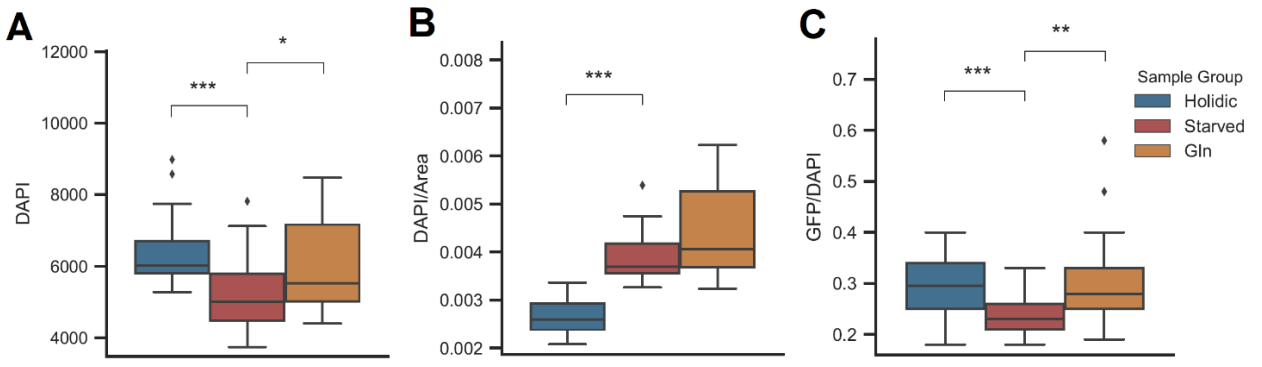

Fig. 12. Total cell numbers. *Cell counts obtained from DAPI-channel.* ***A)*** *Total cell numbers from whole midguts. Improved nutrition was seen to increase cell numbers, most prominently in holidic group. The Gln group was found to grow in cell numbers, but also has a greater variance than holidic group.* ***B)*** *The well-fed midgut has significantly fewer nuclei per area. This is mostly due to enlargement of cytoplasm. The Gln supplementation was found to affect the cell numbers, but the effect is not statistically significant per unit of area.* ***P-values: * ≤ 0.05; ** ≤ 0.01; *** ≤ 0.001.***

distances between nuclei (Fig. 13A,B). Accordingly, while most of the cell populations are larger in the holidic group, its cell densities are lower. Intriguingly, the addition of high dose of Gln to the diet seems to have driven a proliferation increase similar to holidic group. The total cell numbers between the two groups were comparable, and the midguts experienced similar growth in fraction of lineage labelled cells (Fig. 12C).

Measurement of the area of the nuclei clearly shows enrichment of larger nucleus sizes in the holidic and glutamine supplemented sample groups (Fig. 13C). The Gln-group's probability distribution histogram of nuclei areas shows increases at around 250–300 μm^2, while the holidic group is heavy-tailed towards larger areas. The probability density distribution of Gln supplemented midgut cells resembles a transitional stage between the starved and well-fed groups. This could be explained by incrementally enhanced calorie and nutrient intake between the sample groups, which leads to ploidy increases.

The transition boundaries between regions were not always clear with a microscope but could be observed when plotted by average distance between closest nuclei. The transitional regions typically have smaller, more densely packed cells. Again, due to increase in cytoplasm volume the average distances are greater in well-fed midguts. For the most part, there is no real difference in the average distances between the control and Gln supplemented groups. Notably, in the R3-region at positions

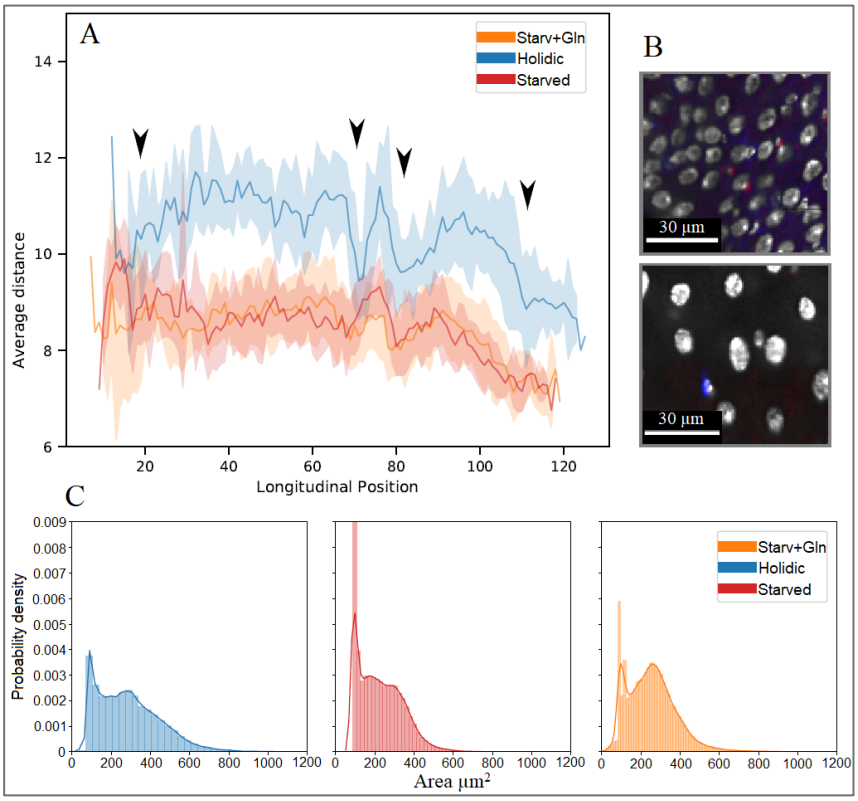

Fig. 13. Cell size–related data from LAM. A) *the average minimum distance between two nearest nuclei. Nutritional status greatly affects the volume of cytoplasm. Lines are the average between two closest cells and bands are standard deviation. Arrows show transitions between regions.* ***B)*** *comparison of cell density between starved and holidic sample groups. The difference cytoplasm volume is very distinguishable in microscopy images. Upper is starved and bottom holidic.* ***C)*** *histograms of cell nucleus sizes by sample group. Compared to the control group, the more nutritious diets show heavier tails and right-shifted peaks, i.e. increased nucleus sizes.*

70–80 of the Gln-group, the average distances dropped. This was due to regional increase in cell numbers (see 5.2.1).

increased nutrition grew the length of the midguts as expected. The lengths of the midguts as measured by vector length were 4.78 ± 0.63 mm for holidic, 3.58 ± 0.37 mm for starved, and 3.97 ± 0.47 mm for Gln-group. In addition to the holidic group's growth in length and cytoplasm volume, a change in the overall proportion of anterior and posterior midgut was detected. This presents itself as relatively elongated posterior and shortened anterior (see Fig. A 7). The proportional change was approximated by determining the number of bins between the R3 and R4/5 –MPs. For all sample groups, the average bin location of R4/5–MP was 90, compared R3–MP bin of 55 ± 4, 61 ± 4, 60 ± 5 for holidic, starved, and Gln groups respectively. As the R4/5-boundary stayed at the same bin

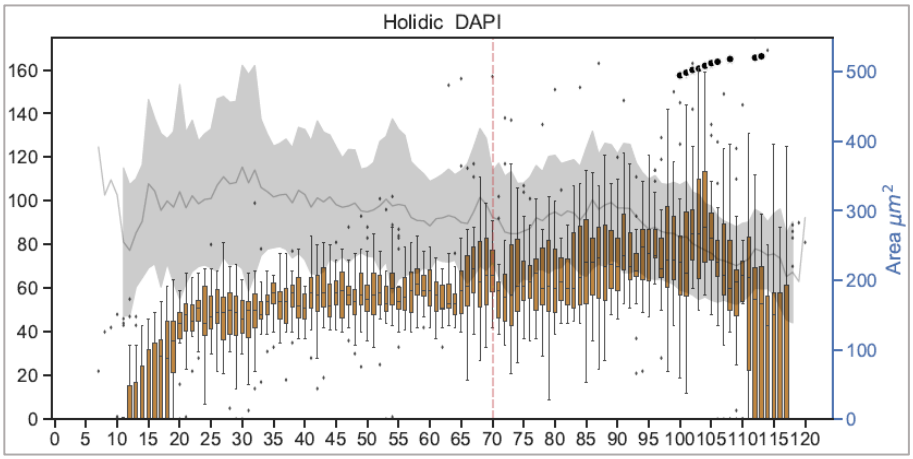

Fig. 14. Holidic total nuclei and average nucleus area. *The box plot contains the 100 bins obtained from 19 samples by LAM and indicates total nucleus counts. The line is the average nucleus area at each bin location, and the band is standard deviation. The total cell numbers increase from anterior to posterior, while the average area decreases at a comparable rate. The top-right markers show the spread of secondary measurement points at R4/5-boundary.*

between the samples, the relative growth must be limited to R4 and posterior R3. Therefore, the average length of the posterior midgut up to the R4/5-boundary is on average six bins greater in holidic samples than in starved samples, corresponding to a relative increase of approximately 20%. Accordingly, the R1 and R2 regions were relatively smaller. The same effect was also seen in Gln-group, albeit to almost non-existing degree.

The average total cell number per bin was found to slowly increase along the longitudinal axis within all groups, with regional declines at the boundary of R2 and R3 (Fig. 14). In contrast, the average nucleus sizes tended to have a slight downward slope from anterior to posterior. A similar result was seen in the average distances between nuclei: the cells are more constricted in the posterior midgut. While glutamine had an overall effect promoting growth of nucleus size, its result was not localised and can therefore be deemed midgut-wide.

5.2 Variation in Cell types

Variations in cell populations were apparent between the sample groups. The cell populations were typically found to be largest in the holidic diet group, as was expected. Lineage labelled cells increased significantly from anterior to posterior in holidic group, and in Gln group from middle-

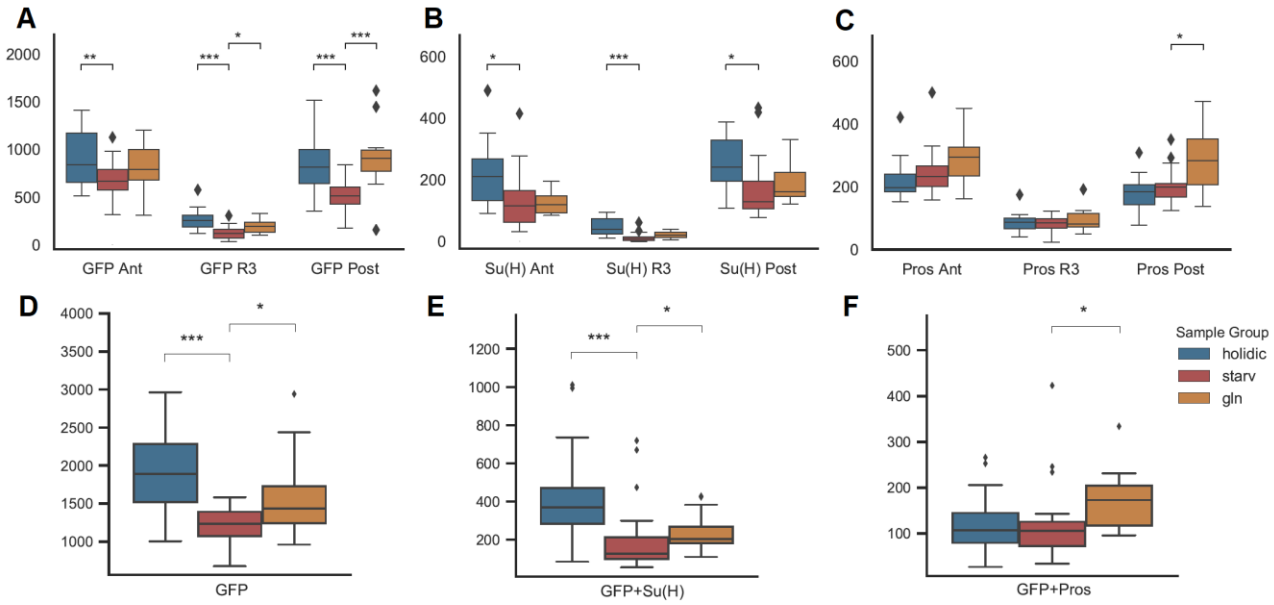

Fig. 15. Numbers of cells by type and location on anterior/middle/posterior-compartmentalisation. A) *Total lineage labelled cells per location. Gln supplementation increased cell numbers primarily within the middle and posterior midgut, while holidic group saw increases in whole midgut.* ***B)*** *Enteroblasts were found to be significantly increased only within holidic group.* ***C)*** *Minor increases of EE numbers can be seen along the midgut, but greatest and significant increase was in the posterior part.* ***D)*** *Total whole-midgut lineage labelled cells were significantly increased in both holidic and Gln groups.* ***E)*** *Total lineage labelled EBs were also found to be significantly increased in both groups.* ***F)*** *Only Gln group showed significant increases in lineage labelled EEs.* ***P-values: * ≤ 0.05; ** ≤ 0.01; *** ≤ 0.001.***

region (p=0.012) to posterior (p=0.0003, Fig. 15A). These increases in GFP$^+$ cells show that the diet regimens activated proliferation within the groups in comparison to control. The Gln supplementation was found to increase total numbers of all cell types significantly, except for Su(H) positive enteroblasts. On the other hand, minor but significant increases were detected in lineage labelled EBs, i.e. GFP+Su(H) (p=0.011, Fig. 15E). The amount of enteroendocrine cells was found to be nearly constant between starved and holidic-fed midguts with 503±120 and 495±108 EEs in total, respectively. In contrast, Gln supplementation significantly increased EE numbers to 649±159 per midgut, an increase of nearly 30% (p=0.047). Accordingly, the total number of lineage labelled EEs was also found to rise significantly (p=0.028, Fig. 15F).

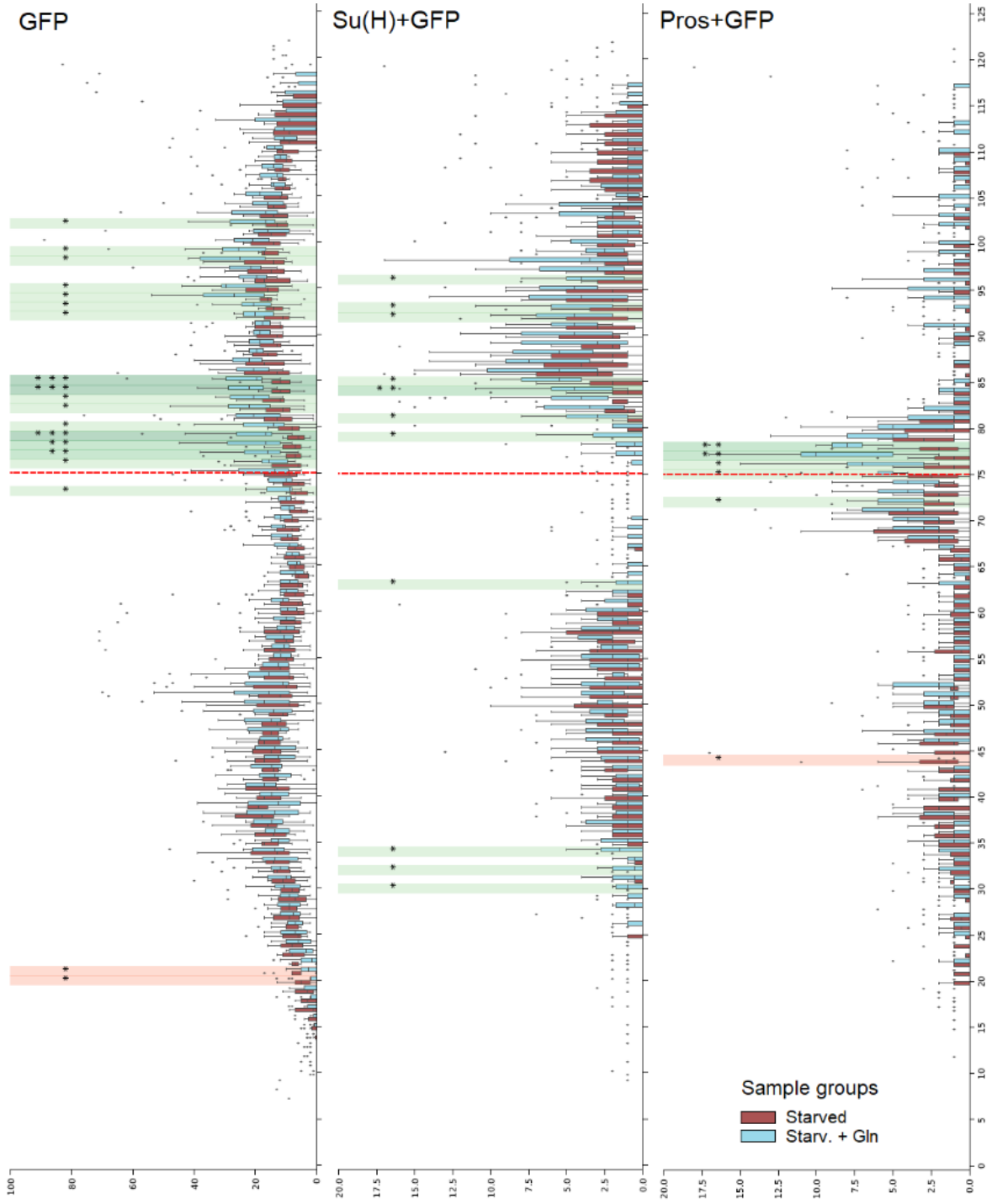

Fig. 16. Statistics between the glutamine supplemented and starved sample groups. *The effects of glutamine can mostly be seen to the posterior from R3. GFP-positive EEs were greatly increased in posterior R3. For GFP$^+$ EBs, proliferation can be seen in transitional boundary between R3 and R4, and anterior R4. Y-axis indicates position from anterior to posterior. Green color indicates significantly higher values than in the control group, red significantly lower. The R3-midpoint is at Y=75, indicated by dashed red line. Asterisks on the left side denote* ***p-values: * ≤ 0.05; ** ≤ 0.01; *** ≤ 0.001.***

5.2.1 Regional Differences

The high resolution of LAM specified significant regional changes in cell populations. Lineage labelled, or GFP^+ cells, were found to be increased in posterior R3 and anterior R4 by Gln supplementation (). Accordingly, within the same regions both Prospero and Su(H) positive cells were found to be increased, albeit in a minor way for the $Su(H)^+$ EBs. In contrast, the holidic diet activated ISC proliferation that lead to increases in the GFP^+ EBs nearly throughout the whole midgut (Fig. A 6). Most of the increase in the Gln group was seen in the near vicinity of the transitional boundary between R3 and R4. Within this 15 bin region on samples that contained both Pros and Su(H) channels, the fractions of GFP-positive EE and EB cells were on average 24.6 ± 12.7 % for starved, 30.2 ± 8.5 % for Gln supplemented, and 33.5 ± 16.2 % for holidic group. As the proportions of these cells remained almost the same, it could be deduced that while glutamine increased proliferation, it had no clear effect on the ratio of asymmetric and symmetric divisions of the ISC. However, the proportion of GFP^+–EE cells compared to total GFP-positive cells in the region increased from 11.3 ± 12.6 % in control group to 15.1 ± 6.2 % in the glutamine supplemented group. Overall, these data imply that glutamine supplementation positively and region-specifically affected the differentiation rate of $Pros^+$ ISCs into EEs.

Interestingly, while glutamine supplementation led to increased progenitor activity in posterior R3 and anterior R4, in the anterior R3 only EEs increased in a significant manner. This supports the notion of separate functional identities between the subregions within R3. Most of the cell number increase in the anterior R4 was attributed to greater numbers of GFP^+ EBs. In the holidic media, the activation of proliferation was evident in the anterior "stomach"–R3 -region, as named by Strand and Micchelli (Strand and Micchelli, 2011). To reiterate, this effect was not present in the Gln samples. Contrastingly, the holidic diet-fed guts did not have increased numbers of EE in the R3, suggesting a Gln-specific effect.

For the most part, the effects of glutamine supplementation did not align with the changes detected in the holidic group (Fig. 17). Consequently, it could be posited that much of the acquired changes are attributable to dose-dependent glutamine effects. The effects of the holidic diet can be seen in several areas along the midgut, while the glutamine supplementation has more localised effects.

The full statistical comparison plots between sample groups can be found in Appendix C (Fig. A 2).

5.3 Result Summary

In contrast to the control group, the other groups were found to grow midgut area and length, and to increase proliferation. The growth was most evident in the holidic group, as was expected. Additionally, improved nutrition was found to alter the proportions of anterior and posterior midgut lengths. A clear inverse relation was found between cell numbers and nucleus size, with larger nuclei in the anterior and smaller in the posterior, and vice versa for the cell numbers. In contrast to the other groups, the holidic diet also caused cells to greatly expand cytoplasm volume.

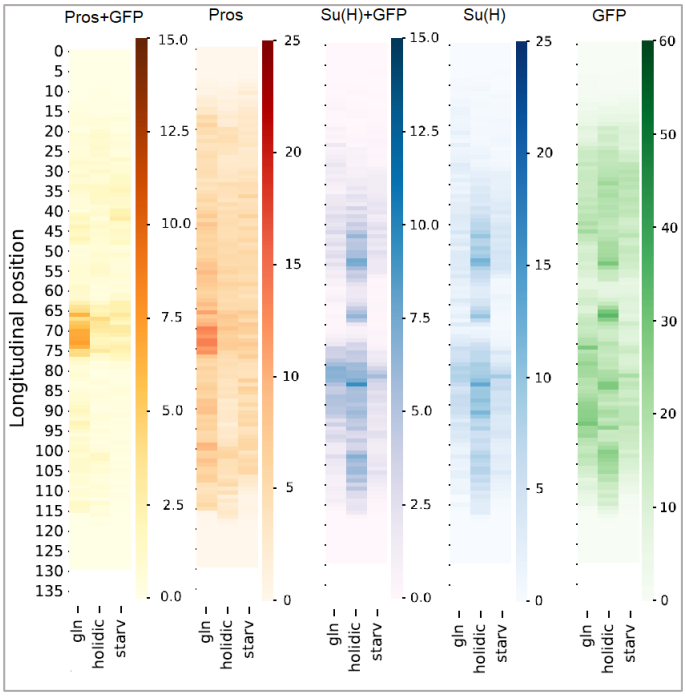

Fig. 17. Heatmaps of cell counts. *The data are bin cell count averages for each sample group. The effects of Gln can be seen mostly located from the middle-region to the mid-posterior. The holidic group has comprehensive changes. It is notable that the effects of glutamine do not in large align with the regions of increase in the holidic group.*

The Gln supplementation led to total cell number increases comparable to holidic group. with greatest increases localised at posterior R3 and anterior R4. This local surge in numbers can be mostly attributed to GFP-positive cells, mainly GFP^+ EEs. The holidic group experienced great increases of GFP^+ EBs in several areas. Gln supplementation was also found to have activated limited endocycling. Additionally, the holidic diet induced a nutrient-dependent activation of GSC at the R3–"stomach" that was not present in Gln samples.

6. Discussion and Future Prospects

The midgut of *Drosophila* has been found to be an highly adaptable organ that responds to feeding or starvation by either driving proliferation, activation of metabolical pathways, and overall growth, or vice versa (Choi et al., 2011; O'Brien et al., 2011). How specific nutrients induce these changes and regulate different nutrient-dependent pathways are still under study. At the heart of the activation of the midgut are the intestinal stem cells that are liable for the replenishment of the cells within the midgut. The regionalisation of the midgut adds a layer of complexity within the mechanisms found in the midgut (Buchon et al., 2013; Marianes and Spradling, 2013). Previous studies to nutrient-induced stem cell activation have mainly focused on subsections of the midgut, or have not considered each region separately, and may consequently have not revealed the full extent of stem cell activation (Choi et al., 2011; O'Brien et al., 2011; Zeng and Hou, 2015). In this thesis, the effects of glutamine supplementation on the cell populations of the midgut were studied using an unprecedented region-by-region whole midgut analysis.

The nutrient-dependent growth of midguts in nutrient-replete conditions is well documented (Choi et al., 2011; Lemaitre and Miguel-Aliaga, 2013; O'Brien et al., 2011). In accordance to the literature, overall growth in cell numbers and midgut length and area was detected in the well-fed guts. Similarly, Gln supplementation was found to increase proliferation to comparable levels with holidic diet, yet midgut size growth remained minimal in comparison to holidic diet. In mammalian models, glutamine has been shown to enhance the effects of several growth factors, such as epidermal growth factor (EGF) and insulin-like growth factor (IGF) (Kim and Kim, 2017). Considering that earlier studies show that both IGF and EGF receptor signalling can induce proliferation, they seem likely mechanisms for Gln-induced proliferation (Biteau and Jasper, 2011; Vinayagam et al., 2016). While the midguts on holidic diet grew in length on average by more than 30 % and their surface areas nearly doubled compared to starved midguts, the acquired ~20 % increase in total cell numbers could seem quite low. However, these results highlight the well-documented role of endoreplication and cell size increase in the nutrient availability–dependent responses of the midgut (Choi et al., 2011; Zielke et al., 2013).

Interestingly, while no cellular hypertrophy was detected in the Gln supplemented midguts, a limited activation of endoreplication was detected in the ECs. Judging solely on the area probability plots,

the endoreplication seems to have been restricted to increased numbers of ECs with DNA content of 4–8N, as the starved and Gln supplemented samples have similar distribution in the larger nucleus sizes (Fig. 13C). A previous study by Choi *et al.* described EC endoreplication to be limited by protein-content of diet and to be dependent of insulin signalling (Choi et al., 2011). In human melanoma cells, inhibiting Gln transport has been found suppress proliferation and decrease expression of Cyclin-dependent kinase 1 (Cdk1) (Wang et al., 2014). Considering that in *Drosophila* the down-regulation of Cdk1 has been deemed necessary for endoreplication, it is surprising that increased glutamine in diet would promote endoreplication (Zielke et al., 2013). However, regulation in cancer cells cannot often be transferred to normal cells. Additionally, as the endoreplication was limited in scope, its regulation must be more complex, and the increase could be from a dose-dependent amino acid content of the diet. Future studies could investigate if this result can be replicated with other amino acids.

Glutamine-induced effects in proliferation were mostly seen in the posterior half of the midgut. This is in accordance to earlier literature, where the posterior midgut has been designated to have the most active stem cells, at least regarding nutrient-dependent adaptive growth (Losick et al., 2011; O'Brien et al., 2011; Ohlstein and Spradling, 2006). Greatest cell number increases in the Gln supplemented midguts was detected at the posterior R3, where glutamine triggered a region-specific increase in numbers of EE cells that was not present in the control group or the holidic sample group. This indicates a dose-dependent effect as the holidic diet also contains glutamine at a relatively very low level. In humans, glutamine has been found to increase proliferation of autophagy-related genes (Kim and Kim, 2017). In the *Drosophila* intestine, expression of autophagy gene *atg16* has been associated with EE differentiation through Slit/Robo signalling, suggesting a possible mechanism for glutamine-induced cell-fate determination. However, the increase in EE population may be exaggerated due to noisiness of the labelling dye on some Gln-fed midguts.

The approximate R3–R4 area that experienced the greatest growth in cell populations is incidentally characterized by Buchon *et al.* to uniquely express for example Magro, which is a sterol esterase (Buchon et al., 2013). It is known that Gln is a regulator of sterol regulatory element-binding proteins in humans, and that insects are not able to synthesize sterols and consequently need them from diet (Inoue et al., 2011; Lemaitre and Miguel-Aliaga, 2013). It has also been shown that the posterior ECs have overall enriched expression of genes involved in lipid metabolism (Marianes and Spradling,

2013). Additionally, the EE secrete multiple lipid metabolism–related hormones, such as tachykinins that are involved in lipid homeostasis and are produced in large quantities (Song et al., 2014). Intriguingly, a recent study found that dietary lipids modulate Notch-signalling during the first several days as an adult to determine the ultimate numbers of EE within the posterior midgut (Obniski et al., 2018). This modulation was dependent on Hr96, a nuclear hormone receptor important for lipid metabolism that also regulates genes related to sterol metabolism. Taken together, these evidences beg the question whether Gln supplementation might have activated pathways related to lipid metabolism, subsequently leading to cell number increases, and most importantly to activation of differentiation into EEs. However, lipid-dependent regulation of midgut homeostasis is not well-studied, and the question whether the increased differentiation into EEs could be due to lipid metabolism and/or autophagy-related expression remains unanswered.

The detected inverse relation between nucleus sizes and cell numbers could indicate that the anterior enterocytes have a higher rate of endocycling than their counterparts in the posterior midgut. The same effect was also seen in the average distance between nuclei, which functions as a proxy to cytoplasm volume. These data could be taken as evidence for the anterior midgut's greater role in the secretion of digestive enzymes: the greater polyploidy allows for increased expression of related genes, and subsequently also leads to increased volume (Choi et al., 2011; Miguel-Aliaga et al., 2018). The posterior midgut on the other hand serves as the main absorptive region (Miguel-Aliaga et al., 2018). Interestingly, the length of posterior midgut was found to grow relative to anterior midgut with improved nutrition. As nutrient absorption is dependent on the luminal surface area, the detected growth in the length of the midgut is evolutionarily sensible.

Overall, glutamine was found to clearly increase ISC proliferation, supporting the existing literature on the beneficial effects of Gln supplementation on intestinal health (van der Hulst et al., 1993; Miller, 1999; Moore et al., 2015; Yang et al., 2014). However, some studies into the effects of Gln supplementation on patients have found contradictory results (Kim and Kim, 2017). The specific mechanisms of Gln-induced effects are not well known, and the results of this thesis could give some insight. If Gln supplementation in humans leads to similar increases in EE cells as in midgut, a continued supplementation could lead to disbalance in the enteroendocrine system, subsequently leading to unforeseen effects. Studying the extent of EE differentiation in flies on a long-term Gln supplementation could shed some light on the question.

Overview of LAM

The error rate of LAM increases with every further bin from the sample group anchoring point, i.e. the R3–MP. This is unavoidable, as nutrition was found to affect the proportions of the midgut. As the analyses for this study were performed with a single vector encompassing the whole midgut for each sample, the terminal ends in both anterior and posterior do not necessarily align between sample groups. This was most clearly seen in comparison of nuclei counts between starved and holidic-fed midguts (Fig. A 7). While this study used one vector for whole midgut, LAM can be used to analyse multiple smaller regions of the midgut in sequence, consequently lowering the compounding error rate from proportional variation.

LAM has limitations regarding the vector creation: inordinate curvature of midgut hampers the calculation of the running median. In this regard, the proper mounting of the midgut is paramount. Additionally, while the microscope image intensity features may be analysed in three dimensions, the vector creation is constrained to planar geometries by the Shapely-package, which could pose complications in some experiments. Development of alternative methods of vector creation could be useful for some experiments.

The similarity of the data and plots between the sample groups speaks for the power of the new analysis method. The effects of varying nutrition can in many channels be seen highly localized. This adds to the well–established proof of regional functionality and separate regulatory mechanisms within the midgut (Buchon et al., 2013; Dutta et al., 2015; Miguel-Aliaga et al., 2018). Overall, LAM enables new possibilities in the research of nutrient control of stem cells within the midgut. Moreover, the method could be either immediately utilized or be readily adapted for many experiments, and possibly different tissues, to measure contrasting properties and variation in cell populations from microscopy images.

7. References

Adams, R., and Bischof, L. (1994). Seeded region growing. IEEE Trans. Pattern Anal. Mach. Intell. *16*, 641–647.

Aghajanian, P., Takashima, S., Paul, M., Younossi-Hartenstein, A., and Hartenstein, V. (2016). Metamorphosis of the Drosophila visceral musculature and its role in intestinal morphogenesis and stem cell formation. Dev. Biol. *420*, 43–59.

Aledo, J.C. (2004). Glutamine breakdown in rapidly dividing cells: Waste or investment? BioEssays *26*, 778–785.

Amcheslavsky, A., Song, W., Li, Q., Nie, Y., Bragatto, I., Ferrandon, D., Perrimon, N., and Ip, Y.T. (2014). Enteroendocrine Cells Support Intestinal Stem-Cell-Mediated Homeostasis in Drosophila. Cell Rep. *9*, 32–39.

Apidianakis, Y., and Rahme, L.G. (2011). Drosophila melanogaster as a model for human intestinal infection and pathology. *30*, 21–30.

Benjamini, Y., and Hochberg, Y. (1995). Controlling the False Discovery Rate: A Practical and Powerful Approach to Multiple Testing. J. R. Stat. Soc. Ser. B *57*, 289–300.

Biteau, B., and Jasper, H. (2011). EGF signaling regulates the proliferation of intestinal stem cells in Drosophila. Development *138*, 1045–1055.

Bitplane Inc (2018). Imaris.

Brand, A.H., and Perrimon, N. (1993). Targeted gene expression as a means of altering cell fates and generating dominant phenotypes. Development *118*, 289–295.

Buchon, N., Osman, D., David, F.P.A., Yu Fang, H., Boquete, J.P., Deplancke, B., and Lemaitre, B. (2013). Morphological and Molecular Characterization of Adult Midgut Compartmentalization in Drosophila. Cell Rep. *3*, 1725–1738.

Choi, N.H., Lucchetta, E., and Ohlstein, B. (2011). Nonautonomous regulation of Drosophila midgut stem cell proliferation by the insulin-signaling pathway. Proc. Natl. Acad. Sci. *108*, 18702–18707.

Clevers, H. (2013). The intestinal crypt, a prototype stem cell compartment. Cell *154*, 274–284.

Cox, J.E., Thummel, C.S., and Tennessen, J.M. (2017). Metabolomic studies in Drosophila. Genetics *206*, 1169–1185.

Duffy, J.B. (2002). GAL4 system indrosophila: A fly geneticist's swiss army knife. Genesis *34*, 1–15.

Dutta, D., Dobson, A.J., Houtz, P.L., Gläßer, C., Revah, J., Korzelius, J., Patel, P.H., Edgar, B.A., and Buchon, N. (2015). Regional Cell-Specific Transcriptome Mapping Reveals Regulatory Complexity in the Adult Drosophila Midgut. Cell Rep. *12*, 346–358.

Fan, J., Zeng, G., Body, M., and Hacid, M.-S. (2005). Seeded region growing: an extensive and comparative study. Pattern Recognit. Lett. *26*, 1139–1156.

Gillies, S., and et al. (2007). Shapely: manipulation and analysis of geometric objects.

Golic, K.G., and Lindquist, S. (1989). The FLP recombinase of yeast catalyzes site-specific recombination in the drosophila genome. Cell *59*, 499–509.

Gramfort, A. (2013). MEG and EEG data analysis with MNE-Python. Front. Neurosci. *7*.

Gramfort, A., Luessi, M., Larson, E., Engemann, D.A., Strohmeier, D., Brodbeck, C., Parkkonen, L., and Hämäläinen, M.S. (2014). MNE software for processing MEG and EEG data. Neuroimage *86*, 446–460.

Guo, Z., and Ohlstein, B. (2015). Bidirectional Notch signaling regulates Drosophila intestinal stem cell multipotency. Science (80-.). *350*, aab0988-aab0988.

Hegedus, D., Erlandson, M., Gillott, C., and Toprak, U. (2008). New Insights into Peritrophic Matrix Synthesis, Architecture, and Function. Annu. Rev. Entomol. *54*, 285–302.

Hensley, C.T., Wasti, A.T., Ralph, J., Invest, J.C., Hensley, C.T., Wasti, A.T., and Deberardinis, R.J. (2013). Glutamine and cancer : cell biology , physiology , and clinical opportunities Find the latest version : Review series Glutamine and cancer : cell biology , physiology , and clinical opportunities. *123*, 3678–3684.

Hughes, T.T., Allen, A.L., Bardin, J.E., Christian, M.N., Daimon, K., Dozier, K.D., Hansen, C.L., Holcomb, L.M., and Ahlander, J. (2012). Drosophila as a genetic model for studying pathogenic human viruses. Virology *423*, 1–5.

van der Hulst, R.R., van Kreel, B.K., von Meyenfeldt, M.F., Brummer, R.J., Arends, J.W., Deutz, N.E., and Soeters, P.B. (1993). Glutamine and the preservation of gut integrity. Lancet (London, England) *341*, 1363–1365.

Hung, R.-J., Hu, Y., Kirchner, R., Li, F., Xu, C., Comjean, A., Tattikota, S.G., Song, W.R., Sui, S.H., and Perrimon, N. (2018). A Cell Atlas of the Adult Drosophila Midgut. SSRN Electron. J.

Inoue, J., Ito, Y., Shimada, S., Satoh, S.I., Sasaki, T., Hashidume, T., Kamoshida, Y., Shimizu, M., and Sato, R. (2011). Glutamine stimulates the gene expression and processing of sterol regulatory element binding proteins, thereby increasing the expression of their target genes. FEBS J. *278*, 2739–2750.

Jiang, H., and Edgar, B.A. (2011). Intestinal stem cells in the adult Drosophila midgut. Exp. Cell Res. *317*, 2780–2788.

Jiang, H., Patel, P.H., Kohlmaier, A., Grenley, M.O., McEwen, D.G., and Edgar, B.A. (2009). Cytokine/Jak/Stat Signaling Mediates Regeneration and Homeostasis in the Drosophila Midgut. Cell *137*, 1343–1355.

Jones, E., Oliphant, T., and Peterson, P. SciPy: Open source scientific tools for Python.

Jonkman, J., and Brown, C.M. (2015). Any way you slice it—A comparison of confocal microscopy techniques. J. Biomol. Tech. *26*, 54–65.

Kim, M.H., and Kim, H. (2017). The roles of glutamine in the intestine and its implication in intestinal diseases. Int. J. Mol. Sci. *18*.

Kong, H., Akakin, H.C., and Sarma, S.E. (2013). A Generalized Laplacian of Gaussian Filter for Blob Detection and Its Applications. IEEE Trans. Cybern. *43*, 1719–1733.

Kretzschmar, K., and Watt, F.M. (2012). Lineage tracing. Cell *148*, 33–45.

Kylsten, P., Kimbrell, D.A., Daffre, S., Samakovlis, C., and Hultmark, D. (1992). The lysozyme locus in Drosophila melanogaster: different genes are expressed in midgut and salivary glands. MGG Mol. Gen. Genet. *232*, 335–343.

Langhorst, M.F., Schaffer, J., and Goetze, B. (2009). Structure brings clarity: Structured illumination microscopy in cell biology. Biotechnol. J. *4*, 858–865.

Lee, N., and Kim, D. (2016). Cancer Metabolism: Fueling More than Just Growth. Mol. Cells *39*, 847–854.

Lee, T., and Luo, L. (1999). Mosaic analysis with a repressible cell marker for studies of gene function in neuronal morphogenesis. Neuron *22*, 451–461.

Lemaitre, B., and Miguel-Aliaga, I. (2013). The Digestive Tract of Drosophila melanogaster. Annu. Rev. Genet. *47*, 377–404.

Losick, V.P., Morris, L.X., Fox, D.T., and Spradling, A. (2011). Drosophila Stem Cell Niches: A Decade of Discovery Suggests a Unified View of Stem Cell Regulation. Dev. Cell *21*, 159–171.

Mann, H.B., and Whitney, D.R. (1947). On a Test of Whether one of Two Random Variables is Stochastically Larger than the Other. Ann. Math. Stat. *18*, 50–60.

Marianes, A., and Spradling, A.C. (2013). Physiological and stem cell compartmentalization within the Drosophila midgut. Elife *2013*, 1–19.

Mattila, J., Kokki, K., Hietakangas, V., and Boutros, M. (2018). Stem Cell Intrinsic Hexosamine Metabolism Regulates Intestinal Adaptation to Nutrient Content. Dev. Cell *47*, 112–121.e3.

McElduff, F., Cortina-Borja, M., Chan, S.-K., and Wade, A. (2010). When t-tests or Wilcoxon-Mann-Whitney tests won't do. AJP Adv. Physiol. Educ. *34*, 128–133.

McKenzie, J.A., and McKechnie, S.W. (1979). A comparative study of resource utilization in natural populations of Drosophila melanogaster and D. simulans. Oecologia *40*, 299–309.

McKinney, W. (2010). Data Structures for Statistical Computing in Python. In Proceedings of the 9th Python in Science Conference, S. van der Walt, and J. Millman, eds. pp. 51–56.

Micchelli, C.A., and Perrimon, N. (2006). Evidence that stem cells reside in the adult Drosophila midgut epithelium. Nature *439*, 475–479.

Miguel-Aliaga, I., Jasper, H., and Lemaitre, B. (2018). Anatomy and physiology of the digestive tract of drosophila melanogaster. Genetics *210*, 357–396.

Mihaylova, M.M., Sabatini, D.M., and Yilmaz, Ö.H. (2014). Dietary and metabolic control of stem cell function in physiology and cancer. Cell Stem Cell *14*, 292–305.

Miller, A.L. (1999). Therapeutic considerations of L-glutamine: A review of the literature. Altern. Med. Rev. *4*, 239–248.

Miller, D.E., Cook, K.R., Arvanitakis, A. V., and Hawley, R.S. (2016). Third Chromosome Balancer Inversions Disrupt Protein-Coding Genes and Influence Distal Recombination Events in Drosophila melanogaster . G3: Genes|Genomes|Genetics *6*, 1959–1967.

Moore, S.R., Guedes, M.M., Costa, T.B., Vallance, J., Maier, E.A., Betz, K.J., Aihara, E., Mahe, M.M., Lima, A.A.M., Oriá, R.B., et al. (2015). Glutamine and alanyl-glutamine promote crypt expansion and mTOR signaling in murine enteroids. Am. J. Physiol. Liver Physiol. *308*, G831–G839.

Myers, E.W., Sutton, G.G., Delcher, A.L., Dew, I.M., Fasulo, D.P., Flanigan, M.J., Kravitz, S.A., Mobarry, C.M., Reinert, K.H.J., Remington, K.A., et al. (2000). The genome sequence of Drosophila melanogaster. Science (80-.). *287*, 2196–2204.

O'Brien, L.E., Soliman, S.S., Li, X., and Bilder, D. (2011). Altered modes of stem cell division drive adaptive intestinal growth. Cell *147*, 603–614.

Obniski, R., Sieber, M., and Spradling, A.C. (2018). Dietary Lipids Modulate Notch Signaling and Influence Adult Intestinal Development and Metabolism in Drosophila. Dev. Cell *47*, 98–111.e5.

Ohlstein, B., and Spradling, A. (2006). The adult Drosophila posterior midgut is maintained by pluripotent stem cells. Nature *439*, 470–474.

Ohlstein, B., and Spradling, A. (2007). Multipotent Drosophila Intestinal Stem Cells Specify Daughter Cell Fates by Differential Notch Signaling. Science (80-.). *315*, 988–992.

Pina, C., and Pignoni, F. (2012). Tubby-RFP balancers for developmental analysis: FM7c 2xTb-RFP, CyO 2xTb-RFP, and TM3 2xTb-RFP. Genesis *50*, 119–123.

Piper, M.D.W., Blanc, E., Leitão-Gonçalves, R., Yang, M., He, X., Linford, N.J., Hoddinott, M.P., Hopfen, C., Soultoukis, G.A., Niemeyer, C., et al. (2014). A holidic medium for Drosophila melanogaster. Nat. Methods *11*, 100–105.

Reiter, L.T., Potocki, L., Chien, S., Gribskov, M., and Bier, E. (2001). A Systematic Analysis of Human Disease-Associated Gene Sequences In. Genome Res. 1114–1125.

Santos, A.J.M., Lo, Y.-H., Mah, A.T., and Kuo, C.J. (2018). The Intestinal Stem Cell Niche: Homeostasis and Adaptations. Trends Cell Biol. *28*, 1062–1078.

Shaw, D., Gohil, K., and Basson, M.D. (2012). Intestinal mucosal atrophy and adaptation. World J. Gastroenterol. *18*, 6357–6375.

Smith, B.N., Ghazanfari, A.M., Bohm, R.A., Welch, W.P., Zhang, B., and Masly, J.P. (2015). A Flippase-Mediated GAL80/GAL4 Intersectional Resource for Dissecting Appendage Development in Drosophila . G3: Genes|Genomes|Genetics *5*, 2105–2112.

Sokolowski, M.B. (2001). Drosophila: Genetics meets behaviour. Nat. Rev. Genet. *2*, 879–890.

Song, W., Veenstra, J.A., and Perrimon, N. (2014). Control of lipid metabolism by tachykinin in Drosophila. Cell Rep. *9*, 40–47.

Strand, M., and Micchelli, C. a. (2011). Quiescent gastric stem cells maintain the adult Drosophila stomach. Proc. Natl. Acad. Sci. *108*, 17696–17701.

Vinayagam, A., Kulkarni, M.M., Sopko, R., Sun, X., Hu, Y., Nand, A., Villalta, C., Moghimi, A., Yang, X., Mohr, S.E., et al. (2016). An Integrative Analysis of the InR/PI3K/Akt Network Identifies the Dynamic Response to Insulin Signaling. Cell Rep. *16*, 3062–3074.

van der Walt, S., Colbert, S.C., and Varoquaux, G. (2011). The NumPy Array: A Structure for Efficient Numerical Computation. Comput. Sci. Eng. *13*, 22–30.

Wang, Q., Beaumont, K.A., Otte, N.J., Font, J., Bailey, C.G., Van Geldermalsen, M., Sharp, D.M.,

Tiffen, J.C., Ryan, R.M., Jormakka, M., et al. (2014). Targeting glutamine transport to suppress melanoma cell growth. Int. J. Cancer *135*, 1060–1071.

Yang, C., Ko, B., Hensley, C.T., Jiang, L., Wasti, A.T., Kim, J., Sudderth, J., Calvaruso, M.A., Lumata, L., Mitsche, M., et al. (2014). Glutamine oxidation maintains the TCA cycle and cell survival during impaired mitochondrial pyruvate transport. Mol. Cell *56*, 414–424.

Zacharioudaki, E., and Bray, S.J. (2014). Tools and methods for studying Notch signaling in Drosophila melanogaster. Methods *68*, 173–182.

Zeng, X., and Hou, S.X. (2015). Enteroendocrine cells are generated from stem cells through a distinct progenitor in the adult Drosophila posterior midgut. Development *142*, 644–653.

Zielke, N., Edgar, B.A., and DePamphilis, M.L. (2013). Endoreplication. Cold Spring Harb. Perspect. Biol. *5*, 1–15.

8. Appendices

Appendix A: Table of resources

	Name / product	Additional information	Producer
Chemicals etc.	Agar		Biowest
	biotin		Sigma-Aldrich
	BSA		Biowest
	CaCl2·6H2O		Sigma
	Cholesterol		Sigma
	Semolina		-
	CuSO4·5H2O		Sigma
	FeSO4·7H2O		Sigma-Aldrich
	HCl		Sigma
	KH2PO4		-
	l-arginine		Acros Organics
	l-Glutamine		Sigma
	l-histidine		Sigma
	l-isoleucine		Sigma-aldrich
	l-leucine		Sigma
	l-lysine (HCl)		Sigma
	l-methionine		Sigma
	l-phenylalanine		Sigma
	l-threonine		Sigma
	l-tryptophan		Sigma
	l-tyrosine		Sigma
	l-valine		Sigma
	Malt		-
	MgSO4 (anhydrous)		Sigma
	MnCl2·4H2O		Sigma
	Na2HPO4		-
	nicotinic acid		Sigma
	Nipagin		Acros Organics
	paraformaldehyde		Sigma-Aldrich
	Propionic acid		Sigma
	pyridoxine (HCl)		Sigma

	riboflavin		Sigma
	Sodium folate		-
	sodium glutamate		-
	thiamine (aneurin)		Sigma-Aldrich
	Triton		Sigma
	Vectashield		Vector Laboratories
	Yeast extract		BD
	ZnSO4·7H2O		Sigma
Microscopy	Clarity DM6000		Aurox
	Objective	20x/0.7 HC PL APO CS wd=0.59	Leica
	Filters	DAPI-LED CC00401	Leica
		GFP-LED CC00406	Leica
		DsRed-LED CC00403	Leica
		Cy5-LED CC00408	Leica
	Camera	Orca-Flash4.0 V2 sCMOS	Hamamatsu
Software, packages and Algorithms	Imaris		Bitplane
	Python 3.7		
	Numpy		
	Pandas		
	Shapely		
	Seaborn		
	Mne.stats		
	Matplotlib		
Antibodies	anti-β-galactosidase		Capella
	anti-mouse Alexa647		Thermo Fisher Sc.
	anti-Prospero		Hybridoma Bank
	anti-rabbit Alexa568		Thermo Fisher Sc.
Fly stocks	Esg F/O	w; esg-gal4 tub-gal80^{ts} UAS-GFP; UAS-Flp Act>CD2>Gal4	
	EB marker	Su(H)-LacZ; TM6B	

Appendix B: Normal probability plots

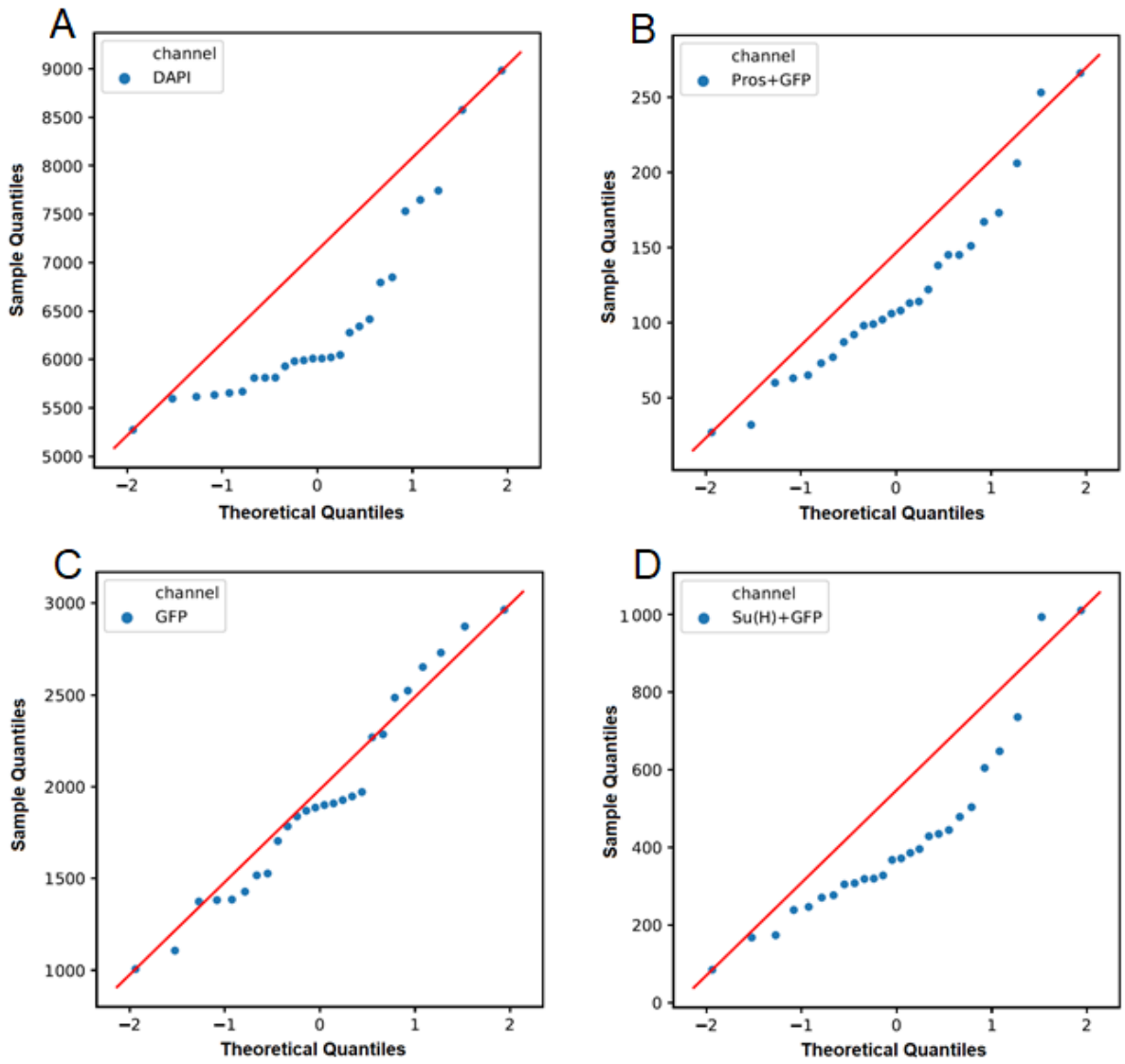

Fig. A 1. Normal probability plots from results of exploratory study. *The observations differ greatly from the theoretical quantiles, i.e. the samples are not normally distributed. For the most part, the data shows right-skewedness (A, B, D), i.e. the distribution's mean is greater than median. As for the GFP-channel, the distribution tends towards uniform (C).*

Appendix C: LAM sample group comparisons

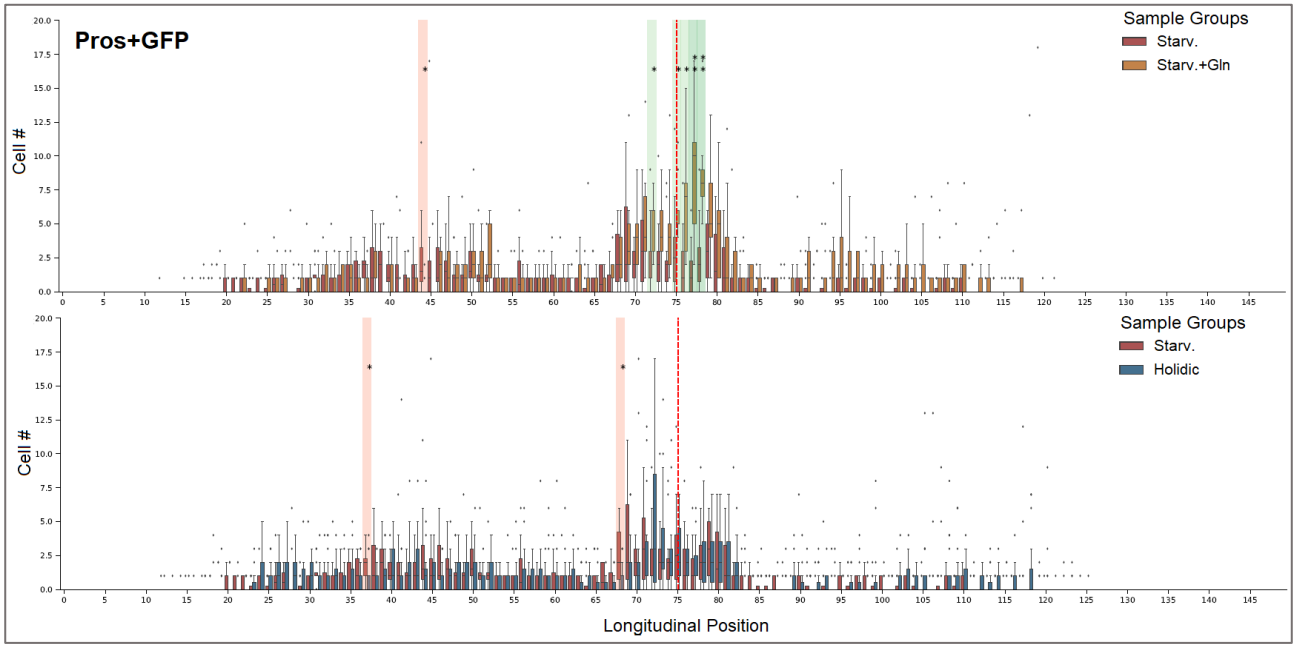

Fig. A 2. Pros+GFP co-localisations. *Compared to the other sample groups, glutamine supplemented midguts have significant increases of EEs in the R3 region.* ***Red and green: lower and higher than control, respectively. P-values: * = 0.05; ** = 0.01; *** = 0.001.***

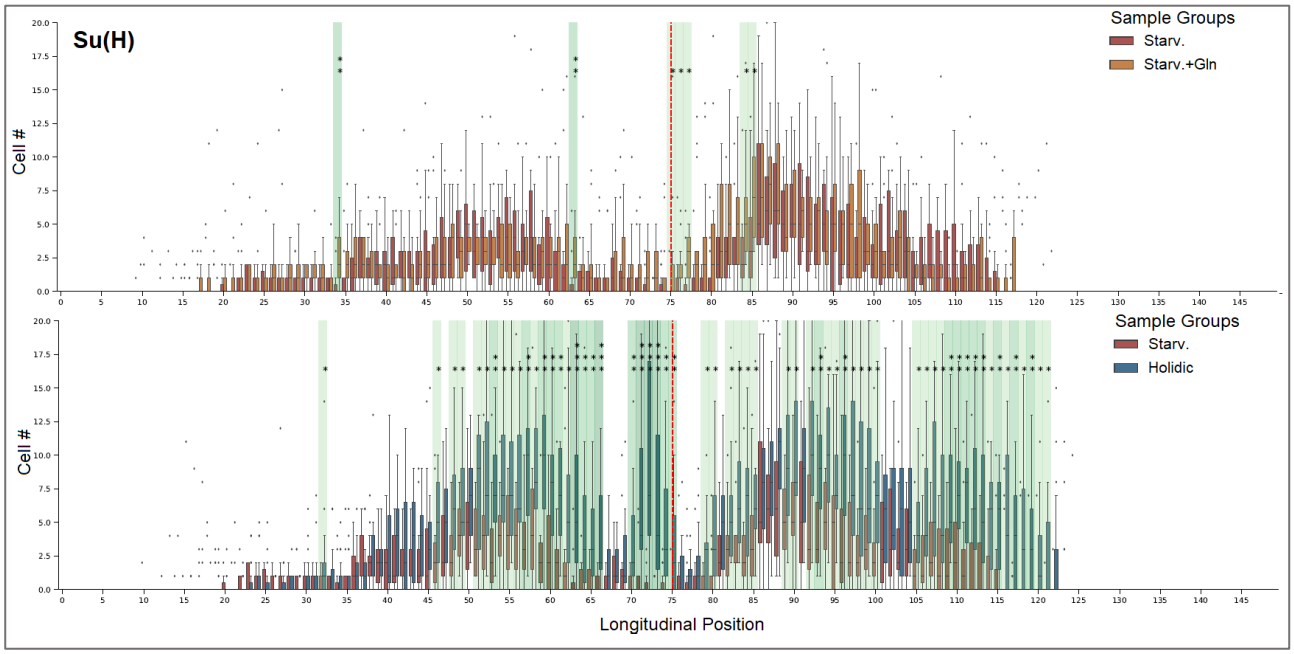

Fig. A 3. Su(H). *Midguts on full holidic diet have greatly more EBs than the others. Notably, anterior R3-region (immediate left from red line) in holidic group has great number of EBs. This has been described in earlier studies and is speculated to enable growth of so-called "stomach" to better handle volumes of food* (Strand and Micchelli, 2011). ***Green: higher than control. P-values: * ≤ 0.05; ** ≤ 0.01; *** ≤ 0.001.***

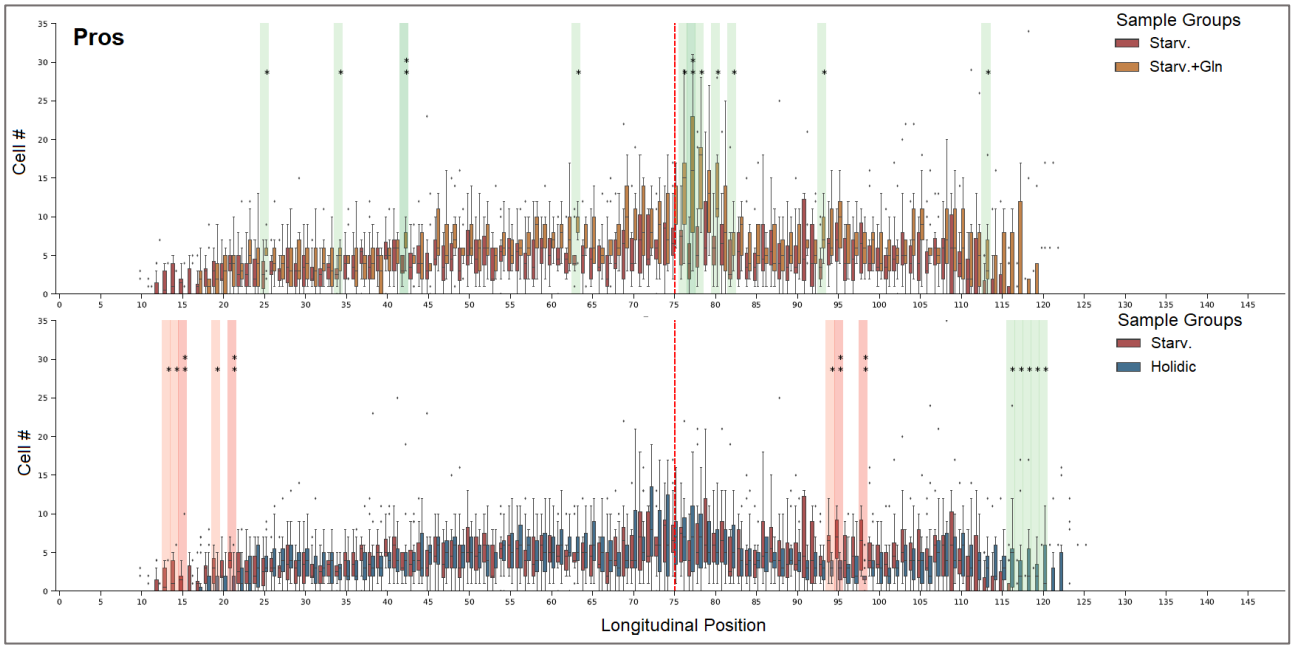

Fig. A 4. Prospero. *Glutamine supplemented have some enrichment of EEs, most notably in R3. The difference of anterior and posterior proportions of starved and fed midguts can be seen easily. i.e. starved midgut has longer anterior part and shorter posterior.* ***Red and green: lower and higher than control, respectively. P-values: * ≤ 0.05; ** ≤ 0.01; *** ≤ 0.001.***

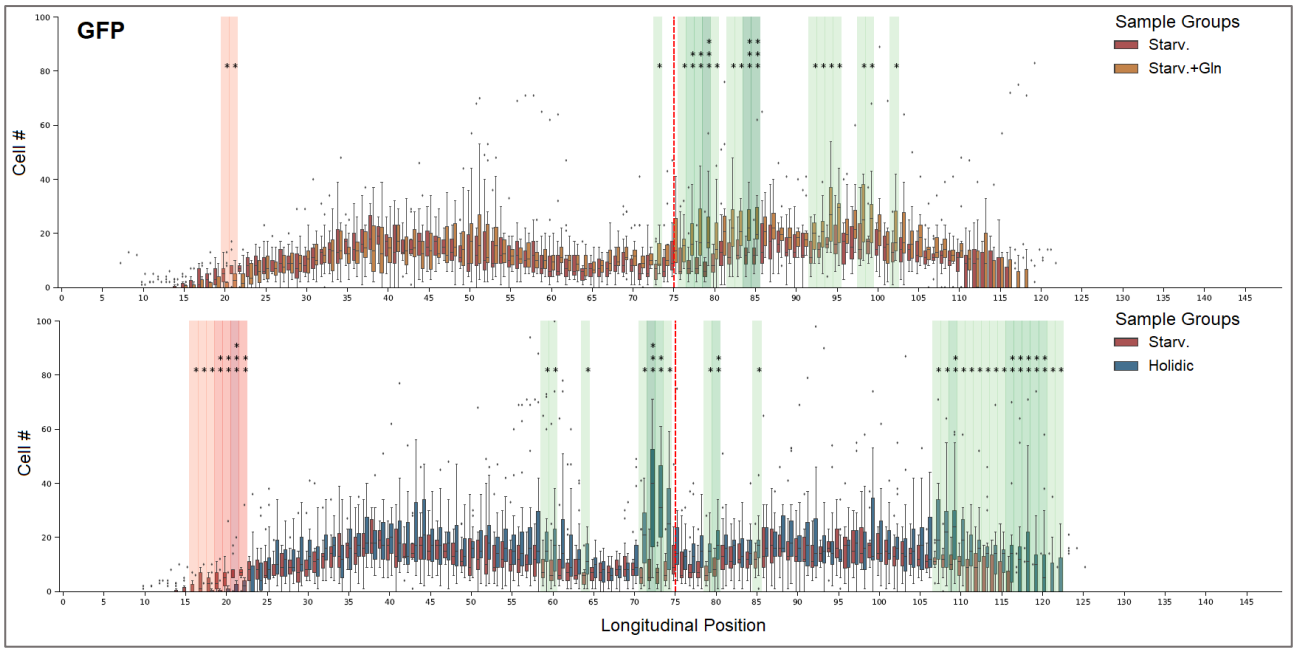

Fig. A 5. GFP. *Significant increases in numbers of ISC and/or EB in the posterior from R3 in the Gln-group. In holidic, the R3- "stomach" can be clearly seen at the anterior–R3. Proportion differences of starved and holidic-groups are evident in anterior and posterior ends.* ***Red and green: lower and higher than control, respectively. P-values: * ≤ 0.05; ** ≤ 0.01; *** ≤ 0.001.***

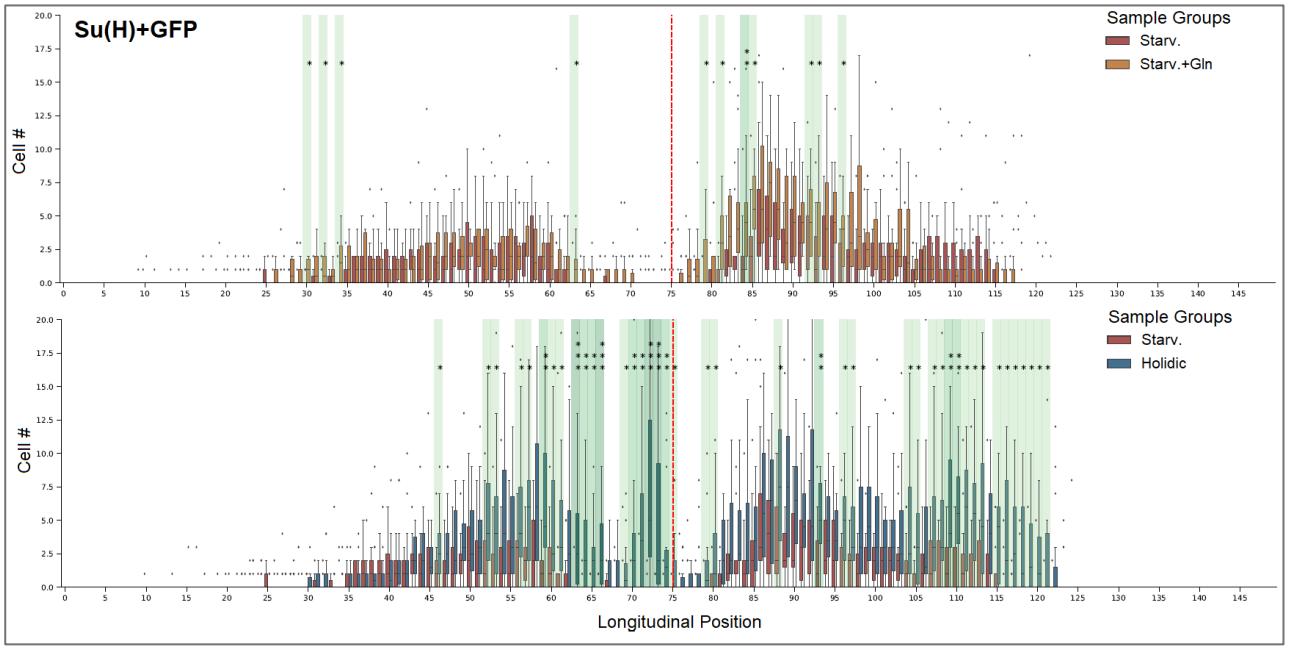

Fig. A 6. Su(H)+GFP co-localisation. *Holidic group has clearly enriched numbers of new EB. Midguts have also responded to glutamine supplementation in a minor manner, best seen in R4.* ***Green: higher than control. P-values: * ≤ 0.05; ** ≤ 0.01; *** ≤ 0.001.***

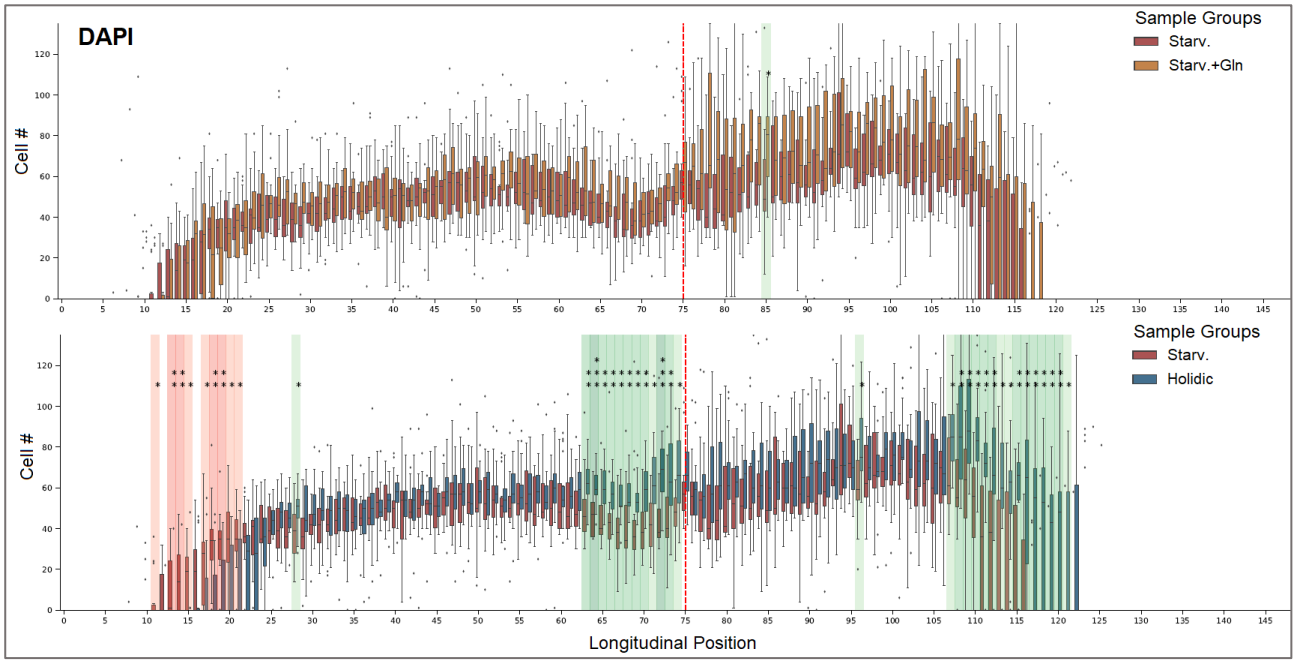

Fig. A 7. DAPI. *Consistent, yet not statistically significant increases in nucleus numbers in the posterior part of Gln-group. Holidic-group has strong enrichment of cells at the R2–3 -border. Anterior and posterior proportion variance between starved and fed are prominent.* ***Red and green: lower and higher than control, respectively. P-values: * ≤ 0.05; ** ≤ 0.01; *** ≤ 0.001.***

HELSINGIN YLIOPISTO
HELSINGFORS UNIVERSITET
UNIVERSITY OF HELSINKI

Appendix D: Growth media

Standard medium

***Table S 1. The standard medium for rearing* Drosophila.**

	INGREDIENT	STOCK	AMOUNT
GELLING AGENT	Agar		44 g
NUTRIENTS	Malt		500 g
	Semolina		260 g
PRESERVATIVES	Propionic acid		46 ml
	Nipagin	100 g/l methyl 4-hydroxybenzoate in 95% EtOH	164 ml
WATER			6400 ml + 400 ml

Measure 6400 ml of water and boil with agar. After, add corn meal and malt in respective order. Boil for 10 minutes mixing occasionally. Warm 400 ml of water to near-boiling, add yeast, mix thoroughly, and then combine. Yeast must not be boiled. Cool down in water bath to under 70 °C and add propionic acid and nipagin. Mix well and add to vials.

Holidic medium

Table S 2. The full holidic growth medium. *First described by Piper* et al. (Piper et al., 2014).

	INGREDIENT	STOCK	PER LITER
GELLING AGENT	Agar		20 g
BASE	Buffer	10×:	100 ml
		30 ml/l glacial acetic acid	
		30 g/l KH_2PO_4	
		10 g/l $NaHCO_3$	
SUGAR	Sucrose		17.12 g
AMINO ACIDS	l-isoleucine		1.82 g
	l-leucine		1.21 g
	l-tyrosine		0.42 g
METAL IONS	$CaCl_2 \cdot 6H_2O$	1,000×: 250 g/l	1 ml
	$CuSO_4 \cdot 5H_2O$	1,000×: 2.5g/l	1 ml
	$FeSO_4 \cdot 7H_2O$	1,000×: 25 g/l	1 ml
	$MgSO_4$ (anhydrous)	1,000×: 250 g/l	1 ml
	$MnCl_2 \cdot 4H_2O$	1,000×: 1 g/l	1 ml
	$ZnSO_4 \cdot 7H_2O$	1,000×: 25 g/l	1 ml
CHOLESTEROL	Cholesterol	20 mg/ml in EtOH	5 ml
	Water (milliQ)		fill to 1l after autoclave

Autoclave 15 min at 120 °C, then sterilely add following:

AMINO ACIDS	Essential amino acid stock solution	8 g/l l-arginine	60.51 ml
		10 g/l l-histidine	
		19 g/l l-lysine(HCl)	
		8 g/l l-methionine	
		13 g/l l-phenylalanine	
		20 g/l l-threonine	
		5 g/l l-tryptophan	
		28 g/l l-valine	
	Nonessential amino acid stock solution	35 g/l l-alanine	60.51 ml
		17 g/l l-asparagine	
		17 g/l l-aspartic acid	
		1 g/l l-cysteine HCl	
		25 g/l l-glutamine	
		32 g/l glycine	
		15 g/l l-proline	
		19 g/l l-serine	
	Sodium glutamate stock solution	100 g/l sodium glutamate	15.13 ml
VITAMINS	Vitamin solution	125×:	14 ml
		0.1 g/l thiamine (aneurin)	
		0.05 g/l riboflavin	
		0.6 g/l nicotinic acid	
		0.775 g/l Ca pantothenate	
		0.125 g/l pyridoxine (HCl)	
		0.01 g/l biotin	
	Sodium folatee	1,000×: 0.5 g/l	1 ml
OTHER NUTRIENTS		125×:	8 ml
		6.25 g/l choline chloride	
		0.63 g/l myo-inositol	
		8.13 g/l inosine	
		7.5 g/l uridine	
PRESERVATIVES	Propionic acid		6 ml
	Nipagin	100 g/l methyl 4-hydroxybenzoate in 95% EtOH	15 ml

Starvation and glutamine media

Table S 3. The starvation and glutamine growth media. *The glutamine medium is otherwise as starvation medium but includes the addition of glutamine after autoclaving.*

	INGREDIENT	STOCK	PER LITER
GELLING AGENT	Agar		10 g
SUGAR	Sucrose		21.4 g
		Water (milliQ)	fill to 1l after autoclave

Autoclave 15 min at 120 °C. For glutamine media, sterilely add following after autoclave:

AMINO ACIDS		l-glutamine	20 g

Appendix E: Imaris Spots–creation parameters

Table S 4. Imaris Spots–creation parameters for different channels. *Background subtraction was used on more noisy channels to more effectively detect cells in noisy areas. Region growing was used for DAPI-channel to find areas and volumes of the nuclei. The axis values are expected diameters of the cells in µm.*

Channel	*x-axis*	*y-axis*	*z-axis*	*Background subtraction*	*Region growing*
DAPI	5.0	5.0	6.0	No	Yes
GFP	5.0	5.0	6.0	Yes	No
Pros	5.0	5.0	10.0	Yes	No
Su(H)	5.0	5.0	10.0	Yes	No